International Journal of Solids and Structures 50 (2013) 4305–4319

Contents lists available at ScienceDirect

International Journal of Solids and Structures

journal homepage: www.elsevier.com/locate/ijsolstr

# Stress-function variational method for interfacial stress analysis of adhesively bonded joints

Xiang-Fa Wu *, Youhao Zhao

*Department of Mechanical Engineering, North Dakota State University, Fargo, ND 58108, USA*

ARTICLE INFO

*Article history:*
Received 23 April 2013
Received in revised form 6 August 2013
Available online 8 September 2013

*Keywords:*
Adhesively bonded joints (ABJs)
Interfacial stresses
Thermomechanical stresses
Free-edge stress
Energy method
Elasticity

ABSTRACT

High interfacial stresses at the free edges of adherends are responsible for the debonding failure of adhesively bonded joints (ABJs). In this paper, a general stress-function variational method is formulated to determinate the interfacial shear and normal (peeling) stresses in ABJs in high accuracy. By extending authors' prior work in stress analysis of bonded joints (Wu and Jenson, 2011), all the planar stress components in the adherends and adhesive layer of an ABJ are expressed in terms of four unknown interfacial stress functions, which are introduced at the upper and lower surfaces of the adhesive layer. A set of governing ordinary differential equations (ODEs) of the four interfacial stress functions is obtained via minimizing the complimentary strain energy of the ABJ, which is further solved by using eigenfunctions. The obtained semi-analytic stress field can satisfy all the traction boundary conditions (BCs) of the ABJ, especially the stress continuity across the bonding lines and the shear-free condition at the ends of adherends and adhesive layer. As an example, the stress field in an adhesively single-sided strap joint is determined by the present method, whose numerical accuracy and reliability are validated by finite element method (FEM) and compared to existing models in the literature. Parameter studies are performed to examine the dependencies of the interfacial stresses of the exemplified ABJ upon the geometries, moduli and temperature change of the adherends and adhesive layer, respectively. The present method is applicable for scaling analysis of joint strength, optimal design of ABJs, etc.



## 1. Introduction

The history of joining technology is as old as our human being itself beginning with building hunting and cultivating tools through binding sharp stones to wood sticks, while use of advanced adhesive bonding techniques in manufacturing modern aircraft structures started only around 30–40 years ago (Davis and Bond, 1999; Higgins, 2000; Park et al., 2010). To date, adhesively bonded metallic joints have been structured in commercial aircrafts with the advent of Airbus A300 (Racker, 2004). Joining technology has also been extended for use in broader primary structures in aerospace, ground vehicles, and other mechanical systems and civil infrastructures. Fig. 1 illustrates several typical adhesively bonded joints (ABJs). By comparison with traditional mechanically fastened bolted, riveted and welded joints, ABJs bear several advantages such as simplified structural design and fabrication, reduced joining space and joint weight, enhanced fatigue tolerance and structural durability, suppression of noises and material wear, and so on (Tomblin and Davies, 2004).

In addition, joining technology also plays a crucial role in microelectronics packaging since 1970s, where thermomechanical stresses have been the leading factor dominating the structural failure and function degradation and have become one of technical concerns (Chen and Nelson, 1979; Suhir, 1989; Eischen et al., 1990; Ru, 2002; Suo, 2003). Accurate prediction of the interfacial thermomechanical stresses in bonded thermostats (chips) is fundamental to understanding the failure mechanism and damage evolution in microelectronic devices subjected to combined mechanical, thermal and electrical loads (Suo, 2003). More recently, flexible electronics based on smart deposition of stiffer silicon micro units onto compliant polymeric substrates become more and more popular, which demands new understanding of their mechanical durability that highly depends on the interfacial stresses near the free edges of the stiff silicon islands (Lu et al., 2007; Kim and Rogers, 2008; Suo, 2012; Sun, 2013). Rapidly expanding utilization of adhesive joining technology in broad engineering sectors also presents new technological challenges to designers, structural analysts and materials scientists such as wise selection of adhesives, accurate strength and durability analysis under various loading and environmental conditions, reliable characterization of structural failure mechanisms, and so on. Among these, accurate stress analysis and rational identification of the failure mechanism and relevant criteria are considered to be crucial.

Substantial progress has been made in theoretical prediction of interfacial stresses in ABJs subjected to either mechanical or

* Corresponding author. Fax: +1 701 231 8913.
*E-mail address:* xiangfa.wu@ndsu.edu (X.-F. Wu).

0020-7683/$ - see front matter © 2013 Elsevier Ltd. All rights reserved.
http://dx.doi.org/10.1016/j.ijsolstr.2013.09.002

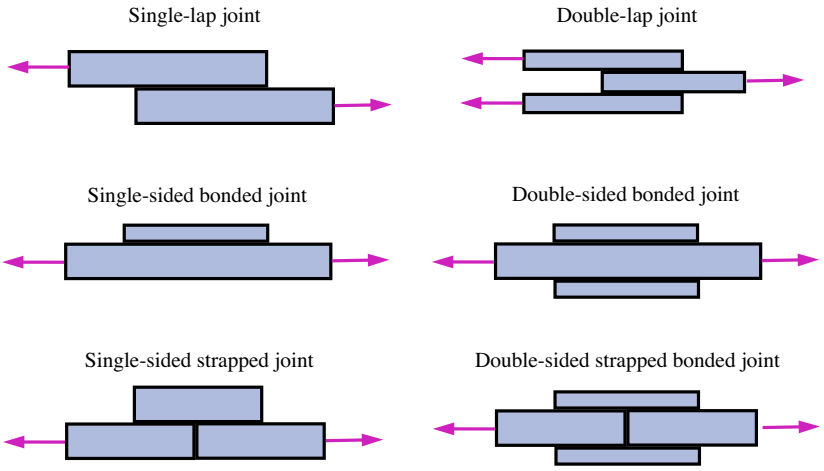


**Fig. 1.** Typical adhesively bonded joints.

thermomechanical loads since the pioneering works by Volkersen (1938) and Goland and Reissner (1944) within the framework of linear elasticity. Yet, limitations still exist in these pioneering joint models and many follow-ups that were mainly induced by their oversimplified assumptions. For instance, the peak shear stresses predicted by Volkersen's and Goland and Reissner's models appear at the adherend ends, which obviously violates the shear-free condition at the free-ends; stress variation across the adhesive layer is assumed very small and ignored, which cannot be held near the adherend ends as to be discussed in this study, etc. In order to enhance the accuracy of stress analysis of ABJs, quite a few modern joint models have been proposed in the last three decades. To mention a few, Delale et al. (1981) formulated an ABJ model, in which the adherends were treated as flexural *Euler–Bernoulli* beams and the deformation of the adhesive layer was ignored due to the small layer thickness. This model was generalized by the authors for stress analysis of all kinds of ABJs. Yet, the shear stress predicted by this model does not satisfy the shear-free condition at the adherend ends; the predicted interfacial stresses are overshot in a large region close to the adherend ends by comparison with those predicted by refined finite element analysis (FEA). Chen and Cheng (1983) further formulated an ABJ model where the stress field in the adherends was expressed in terms of two unknown normal stresses according to two-dimensional (2D) elasticity. These two unknown stress functions were determined by solving a set of two coupled 2nd order ordinary differential equations (ODEs) that were derived by evoking the theorem of minimum complementary strain energy of the joint. Though the stress variation across the adhesive layer was ignored, the stress field gained by this model can satisfy all the traction boundary conditions (BCs). Besides, this model predicted the reasonable location of the peak interfacial shear stress, which was located at a distance of ~20% the adherend thickness from the adherend ends as validated quantitatively by FEA (Mortensen and Thomsen, 2002; Lee and Kim, 2005; Diaz et al., 2009). Furthermore, Tsai et al. (2004) furthered the classic studies by Volkersen (1938) and Goland and Reissner (1944) to adopt a linearly varying shear deformation across the adhesive layer, which can recover the classic Volkersen's and Goland and Reissner's models at the limiting cases. Lee and Kim (2005) considered the adhesively bonded single/double lap joints with the adhesive layers modeled as distributed linearly elastic springs. In addition, there are also a few layerwise models developed recently for stress analysis of ABJs. Hadj-Ahmed et al. (2001) formulated a layerwise model called M4-4N (multi-particle model of multi-layered material with five kinetic fields per layer for an N-layer laminate) for stress analysis of ABJs. In this model, the multi-layers of an ABJ were modeled as a stack of Reissner plates coupled through the interlaminar normal and shear stresses, and the governing equations were obtained via minimization of the strain energy of the ABJ. Diaz et al. (2009) also proposed an improved layerwise ABJ model, in which the ABJ was modeled as a stack of Reissner–Mindlin plates. A set of eight governing ODEs was obtained via evoking the constitutive laws and solved to satisfy the traction BCs. This ABJ model can be well validated by FEM for free-edge interfacial stress prediction. Moreover, Yousefsani and Tahani (2013a,b) recently provided another version of the layerwise ABJ models. In their models, the displacements of artificially divided sub-layers of an ABJ were treated as field variables, and a set of governing ODEs was obtained by evoking the theorem of the minimum potential energy of the joint. For accurate interfacial stress prediction, 18 artificial sub-layers were used in their numerical examples. More detailed survey of the historical developments and comparative studies of several important analytical models for the stress analysis of ABJs and composite joints can be found in the recent review articles by da Silva et al. (2009a,b). Some more recent works include the displacement method (Zhao et al., 2011) for stress analysis of ABJs and stress function method (Kumar and Scanlan, 2013) for stress analysis of adhesively bonded tubular joints with graded interface stiffness, etc. Yet, compared to the perfect theoretical formulation of cracking in layered elastic materials (Suo and Hutchinson, 1990; Hutchinson and Suo, 1992; Yu and Hutchinson, 2001, 2003; Wu and Dzenis, 2002; Wu et al., 2002, 2003), further theoretical refinements are still needed for accurate and efficient stress analysis of ABJs.

Without a doubt, the adhesive layers play a crucial role in all the theoretical modeling of ABJs in the literature, which function to link the adherends of mismatching displacements and physically dominate the structural durability and failure process of ABJs. Yet, mismatch of the material properties between the adherends and adhesive layers has not been rigorously treated or has been oversimplified in most existing models of ABJs though some thermosetting adhesive systems may carry the mechanical properties close to some special adherends made of plastics. In fact, the generalized Hooke's law of the adhesive layers, the shear-free condition at adherend ends, and the stress continuity across the bonding lines of ABJs are normally not satisfied in most literature models of ABJs due to various technical compromises and oversimplifications in modeling. Besides, quite a few misunderstandings still exist in some of the literature models that were mainly induced by oversimplified model assumptions. For instance, some researchers incorrectly claimed that the maximum interfacial shear and normal stresses predicted by their theoretical models

were higher than the values predicted by FEM while not yet realizing the singular nature of these interfacial stresses near the adherend ends such that the numerical values of these stresses could tend to higher and higher with refining the mesh size in FEA. Also, high shear stresses exist at the interfaces between the adhesive layer and adherends near the free-edges, which may lead to a noticeable change of the normal stresses across the adhesive layers even at a very small thickness. Yet, a majority of the ABJ models assume constant shear stress across the adhesive layers. Thus, more sophisticated models are still needed to elucidate the stress nature across the adhesive layers in ABJs, which have been broadly integrated into various engineering structures and systems.

To find more accurate stress field in bonded joints, Wu and Jenson (2011) recently formulated an efficient stress-function variational method. In their formulation, two unknown interfacial shear and normal stress functions were introduced independently, and the stress field in the joint was expressed in terms of the two interfacial stress functions. To simplify the process, the axial normal stress in each adherend of the joint was assumed to be linearly varying across the adherend layer, which is compatible with the flexural stress formula of classic *Euler–Bernoulli* beams as also adopted by many existing joint models. The rest planar shear and transverse normal stresses in the adherends were determined to exactly satisfy the stress equilibrium equations and the traction BCs at the top and bottom surfaces as well as the adherend ends. A set of two coupled governing ODEs of the unknown interfacial stress functions was obtained via triggering the theorem of minimum complimentary strain energy of the entire joint, which was further solved explicitly in terms of eigenfunctions. The stress field obtained by this method has high accuracy and satisfies all the traction BCs and stress continuity across the bonding line, especially the shear-free condition at the adherend ends. It needs to be acknowledged that the concept of such formulation based on minimization of the complimentary strain energy of a bonded joint was initially used by Chen and Cheng (1983), while Wu and Jenson (2011) first introduced two independent interfacial stress functions at the bonding line, which makes the theoretical formulation more straightforward and physically meaningful. Also, such a theoretical framework can be easily extended to other bonded joints including ABJs as to be demonstrated in the present study, adhesively bonded composite and multi-material joints, etc.

Along this vein, in this study we further extend Wu and Jenson's (2011) stress-function variational method to formulate a general semi-analytic method for accurately determining the interfacial stresses in ABJs subjected to mechanical or thermomechanical loads. To demonstrate the efficiency and effectiveness of this method, without loss of generality, we start with a special case of an adhesively single-sided strap joint where two interfaces between the adhesive layer and adherends present. In this case, two unknown interfacial shear and normal (peeling) stress functions can be introduced at each interface. As a result, a set of four coupled ODEs with four unknown interfacial stress functions are obtained after applying the theorem of minimum complimentary strain energy of the joint. Such a set of ODEs can be solved by using eigenfunction method. The rest of the paper is outlined as follows. Section 2 provides detailed formulation of the theoretical framework of stress-function variational method for ABJs. Section 3 demonstrates the effectiveness of the present method in determining the stress field in the model joint subjected to mechanical loads and temperature change, respectively. Detailed parameter studies are performed to explore the dependencies of the interfacial stresses of the model joint upon the geometries, moduli, Poisson's ratios, and temperature change of the adherends and adhesive layer. Comparisons of the present results with those based on FEM and available in the literature are made. Potential applications of the present semi-analytic method and conclusions of the study are addressed in consequence.

## 2. Problem formulation and solution

Without loss of generality, consider an adhesively single-sided strap joint which is made up with two identical slender substrate layers and a slender cover layer, which are adhesively bonded together through a thin adhesive layer as sketched in Fig. 2. The cover layer has the length $2L$, thickness $h_1$, and width $b$; the substrate layers carry the thickness $h_2$, width $b$ and length much larger than $L$; the thickness of the adhesive layer is $h_0$. The coordinate systems are introduced as follows. The $x$-coordinate is selected from the symmetric mid-span of the joint to direct along the layer axis; $y_1$, $y_2$ and $y_0$ are the vertical coordinates with the corresponding origins attached at the centroids of cross-section of the cover, substrate, and adhesive layer, respectively. The substrate layers are subjected to a uniform tensile stress $p_0$ far away the cover layer; meanwhile the joint is subjected to a uniform temperature change $\Delta T$ from the reference temperature of free thermomechanical stresses. Due to symmetry of the joint and external loads, stress analysis of such an ABJ can be made only on the right half-portion (see Fig. 2($b$)). It can be expected that mismatch of the material properties across the adherend interfaces will evoke high interfacial shear and normal stresses (debonding or peeling stresses) at the adherend ends as illustrated in Fig. 2($c$). Such high interfacial mechanical or thermomechanical stresses are responsible for the failure of the ABJs, such as interface debonding as commonly observed in engineered structural ABJs.

In practice, subjected to mechanical or thermomechanical loads, ABJs with finite width are typically in a general three-dimensional (3D) stress state. To simplify the process, hereafter the ABJ is considered in the *plane-stress* state and without residual stresses in the initial load-free state at the reference temperature, and the

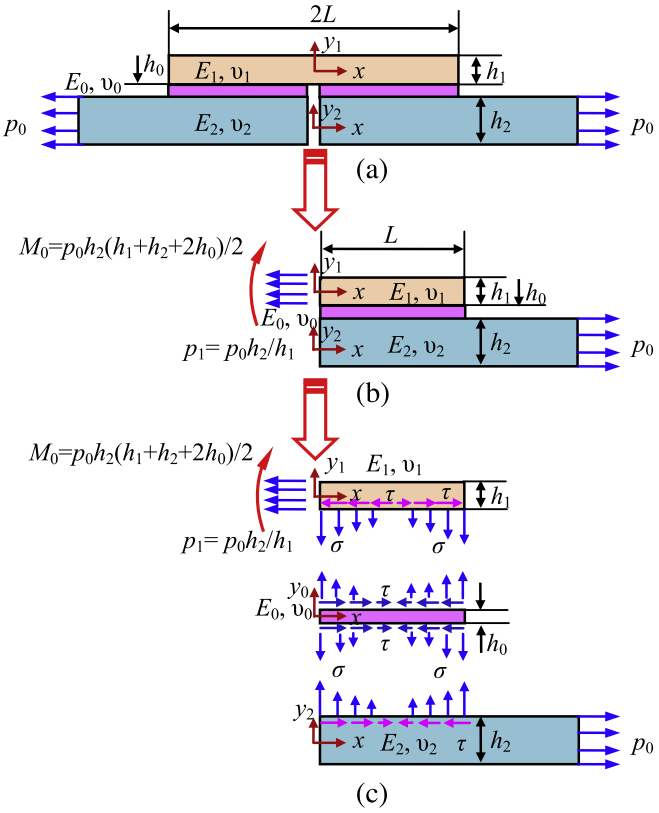


**Fig. 2.** Schematic of a adhesively single-sided strap joint: ($a$) the joint consists of a slender cover layer adhesively bonded to two identical slender substrate layers, ($b$) reduced right half-structure based on symmetry, and ($c$) schematic interfacial shear and normal stresses.

temperature change is assumed to be uniform throughout the joint. In addition, the adherends and adhesive layer are treated as isotropic, linearly thermoelastic solids. Thus, the mechanical and thermomechanical stresses can be treated separately according to method of superposition. For the convenience of derivation, in the following, parameters and variables attached with subscripts 1, 2, and 0 are designated to the cover, substrate and adhesive layers, respectively. Furthermore, results obtained in the *plane-stress* state can be conveniently converted to those in the *plane-strain* state by simply replacing the Young's moduli $E_i(i=0,1,2)$ by $(1-\upsilon_i^2)/E_i$, Poisson's ratio $\upsilon_i(i=0,1,2)$ by $\upsilon_i/(1-\upsilon_i)$, and coefficients of thermal expansion $\alpha_i(i=0,1,2)$ by $(1+\upsilon_i)\alpha_i$.

### 2.1. Static equilibrium equations

Due to loss of lateral symmetry, the deformation of an adhesively single-sided strap joint is a combination of inplanar elongation and lateral deflection. The adherends and adhesive layer of the joint are slender; their axial stresses can be approximated to follow the classic *Euler–Bernoulli beam* theory while the shear and lateral normal stresses are determined to exactly obey the static equilibrium equations in 2D elasticity. Free-body diagrams (FBDs) of the representative segments of the cover, substrate and adhesive layers are plotted in Fig. 3(*a*)–(*c*), respectively, in which the stresses and related stress resultants, i.e., the axial force $S_i$, shear force $Q_i$, and bending moment $M_i(i=0,1,2)$, are defined to follow the standard sign conventions designated in elementary textbooks of *Mechanics of Materials* (Beer et al., 2009). For the representative segmental element of the cover layer (see Fig. 3(a)), the corresponding static equilibrium equations are

$$\Sigma F_x=0: \quad \frac{dS_1}{dx}=-b\tau_1, \tag{1}$$

$$\Sigma F_y=0: \quad \frac{dQ_1}{dx}=-b\sigma_1, \tag{2}$$

$$\Sigma M=0: \quad \frac{dM_1}{dx}=Q_1-\frac{h_1}{2}(b\tau_1). \tag{3}$$

The static equilibrium equations of the representative segmental element of the right substrate layer (see Fig. 3(*c*)) can be expressed as

$$\Sigma F_x=0: \quad \frac{dS_2}{dx}=b\tau_2, \tag{4}$$

$$\Sigma F_y=0: \quad \frac{dQ_2}{dx}=b\sigma_2, \tag{5}$$

$$\Sigma M=0: \quad \frac{dM_2}{dx}=Q_2-\frac{h_2}{2}(b\tau_2). \tag{6}$$

The static equilibrium equations of the representative segmental element of the adhesive layer (see Fig. 3(*b*)) are written as

$$\Sigma F_x=0: \quad \frac{dS_0}{dx}=b(\tau_1-\tau_2), \tag{7}$$

$$\Sigma F_y=0: \quad \frac{dQ_0}{dx}=b(\sigma_1-\sigma_2), \tag{8}$$

$$\Sigma M=0: \quad \frac{dM_0}{dx}=Q_0-\frac{bh_0}{2}(\tau_1+\tau_2). \tag{9}$$

### 2.2. Stress resultants

Define the shear and normal (peeling) stresses at the interface between the upper adherend and the adhesive layer as two independent interfacial stress functions to be determined:

$$\tau_1=f_1(x) \quad \text{and} \quad \sigma_1=g_1(x). \tag{10}$$

Similarly, the interfacial shear and normal (peeling) stresses at the interface between the lower adherend and the adhesive layer are assumed to be another two independent interfacial stress functions to be determined:

$$\tau_2=f_2(x) \quad \text{and} \quad \sigma_2=g_2(x). \tag{11}$$

Thus, the shear-free conditions at the adherend edges at $x=0$ and $L$ stand for

$$f_1(0)=f_1(L)=0 \tag{12a}$$

and

$$f_2(0)=f_2(L)=0. \tag{12b}$$

In addition, the physical conditions of the axial tractions, shear-forces and bending moments at the upper and lower adherend ends as well as at the ends of the adhesive layer specify

$$S_1(0)=p_0bh_2, \tag{13a}$$

$$S_1(L)=0, \tag{13b}$$

$$Q_1(0)=0, \tag{13c}$$

$$Q_1(L)=0, \tag{13d}$$

$$M_1(0)=bm_0=p_0bh_2(h_1+2h_0+h_2)/2, \tag{13e}$$

$$M_1(L)=0, \tag{13f}$$

$$S_2(0)=0, \tag{13g}$$

$$S_2(L)=p_0bh_2, \tag{13h}$$

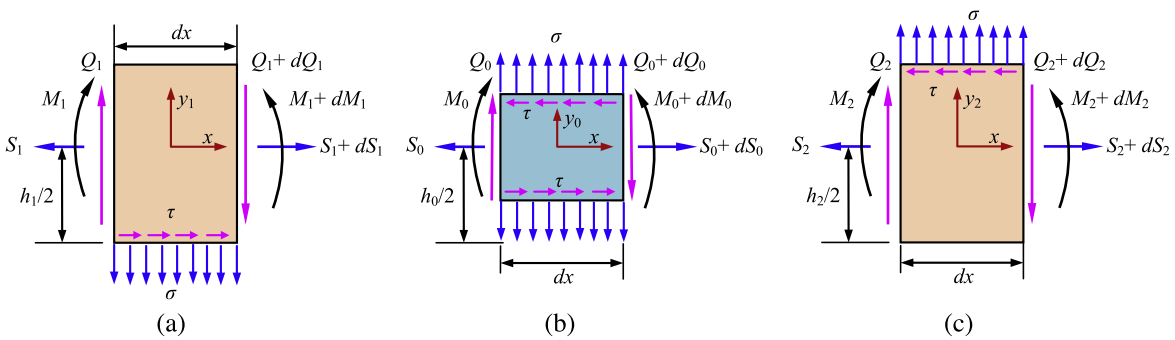


**Fig. 3.** Free-body diagrams of representative segmental elements of the adhesively bonded joint: (*a*) the cover layer, (*b*) the adhesive layer, and (*c*) the right-substrate layer.

$$Q_2(0) = 0, \tag{13i}$$

$$Q_2(L) = 0, \tag{13j}$$

$$M_2(0) = 0, \tag{13k}$$

$$M_2(L) = 0, \tag{13l}$$

$$S_0(0) = 0, \tag{13m}$$

$$S_0(L) = 0, \tag{13n}$$

$$Q_0(0) = 0, \tag{13o}$$

$$Q_0(L) = 0, \tag{13p}$$

$$M_0(0) = 0, \tag{13q}$$

$$M_0(L) = 0. \tag{13r}$$

In the above, not all the traction BCs are linearly independent as will be discussed in Section 2.4.

In the case of thermomechanical stress analysis of the joint due to a pure temperature change $\Delta T$ ($p_0 = 0$), the right terms of (13a), (13e) and (13h) need to be specified as zeros in order to satisfy the traction-free BCs along the axes (without mechanical loads). In this case, the thermomechanical stress analysis of the adhesively single-sided strap joint is equivalent to that of an adhesively bonded thermostat.

Furthermore, stress resultants of all the segmental elements of the layers can be determined completely in terms of the four interfacial stress functions $f_i$ and $g_i (i = 1, 2)$ as follows. By integrating (1) with respect to $x$ from $x = 0$, it yields

$$\int_0^x dS_1 = -\int_0^x b f_1(\xi) d\xi. \tag{14}$$

With the axial force condition at $x = 0$, i.e., BC (13a), the axial normal force (14) in the cover layer can be written as

$$S_1(x) = p_0 b h_2 - b\int_0^x f_1(\xi) d\xi. \tag{15}$$

Integration of (2) with respect to $x$ from $x = 0$ gives the shear-force of the cover layer:

$$\int_0^x dQ_1 = -\int_0^x b g_1(\xi) d\xi. \tag{16}$$

In addition, with the aid of the shear-free condition at $x = 0$ in (13c), the shear-force (16) in the cover layer becomes

$$Q_1(x) = -b\int_0^x g_1(\xi) d\xi. \tag{17}$$

Moreover, integration of (3) with respect to $x$ from $x = 0$ gives

$$\int_0^x dM_1 = \int_0^x \left[Q_1(\xi) - \frac{h_1}{2}(b\tau_1)\right] d\xi. \tag{18}$$

By evoking the bending moment BC at $x = 0$ in (13e), the bending moment (18) in the cover layer can be expressed as

$$M_1(x) = b m_0 - b\int_0^x \int_0^\xi g_1(\varsigma) d\varsigma d\xi - \frac{b h_1}{2}\int_0^x f_1(\xi) d\xi. \tag{19}$$

Based on the same procedure, integration of (4) with respect to $x$ from $x = 0$ yields

$$\int_0^x dS_2 = \int_0^x b f_2(\xi) d\xi. \tag{20}$$

With the axial traction BC at $x = 0$ in (13g), the axial force (20) in the substrate layer can be expressed as

$$S_2(x) = b\int_0^x f_2(\xi) d\xi. \tag{21}$$

Furthermore, the shear-force $Q_2(x)$ and bending moment $M_2(x)$ of the substrate layer can be determined accordingly by integrating (5) and (6) with respect to $x$ from $x = 0$, respectively:

$$Q_2(x) = b\int_0^x g_2(\xi) d\xi, \tag{22}$$

$$M_2(x) = b\int_0^x \int_0^\xi g_2(\varsigma) d\varsigma d\xi - \frac{b h_2}{2}\int_0^x f_2(\xi) d\xi. \tag{23}$$

In the above, the shear-force and bending moment conditions at $x = 0$, i.e., (13i) and (13k), have been triggered. For the adhesive layer, by using the above procedure, integration of (7) with respect to $x$ from $x = 0$ yields

$$\int_0^x dS_0 = \int_0^x b[f_1(\xi) - f_2(\xi)] d\xi. \tag{24}$$

With the axial traction BC at $x = 0$ as given in (13g), the axial force (24) in the substrate layer can be determined as

$$S_0(x) = b\int_0^x [f_1(\xi) - f_2(\xi)] d\xi. \tag{25}$$

Similarly, the shear-force $Q_0(x)$ and bending moment $M_0(x)$ of the adhesive layer can be determined by integrating (8) and (9) with respect to $x$ from $x = 0$, respectively:

$$Q_0(x) = b\int_0^x [g_1(\xi) - g_2(\xi)] d\xi, \tag{26}$$

$$M_0(x) = b\int_0^x \int_0^\xi [g_1(\varsigma) - g_2(\varsigma)] d\varsigma d\xi - \frac{b h_0}{2}\int_0^x [f_1(\xi) + f_2(\xi)] d\xi. \tag{27}$$

In the derivation of (26) and (27), two traction BCs of free shear-force and bending moment of the adhesive layer at $x = 0$ as given in (13o) and (13q) have been implied.

### 2.3. Planar stresses in adherends and adhesive layers

#### 2.3.1. Planar stresses in the upper adherend

For the linearly thermoelastic slender adherends of the ABJ under consideration, as an approach, the axial stress in the adherends can be assumed to vary linearly. Such axial stress can be expressed as the flexural stress according to classic *Euler–Bernoulli beam theory* due to the bending moment superimposed with a uniform axial stress due to pure axial tension. Thus, the axial stress of the cover layer can be expressed as

$$\begin{aligned}\sigma_{xx}^{(1)} &= \frac{S_1}{b h_1} - \frac{M_1 y_1}{I_1} \\ &= p_1 - \frac{1}{h_1}\int_0^x f_1(\xi) d\xi \\ &\quad - \frac{12 y_1}{h_1^3}\left[m_0 - \int_0^x \int_0^\xi g_1(\varsigma) d\varsigma d\xi - \frac{h_1}{2}\int_0^x f_1(\xi) d\xi\right],\end{aligned} \tag{28}$$

where $p_1 = p_0 h_2 / h_1$. Shear stress $\tau_{y_1 x}^{(1)}$ of the cover layer can be determined by integrating the 2D static equilibrium equation of a representative differential element:

$$\frac{\partial \sigma_{xx}^{(1)}}{\partial x} + \frac{\partial \tau_{y_1 x}^{(1)}}{\partial y_1} = 0, \tag{29}$$

with respect to $y_1$ from an arbitrary location $y$ to the top surface at $y_1 = h_1/2$:

$$\int_{y_1}^{h_1/2} \frac{\partial \sigma_{xx}^{(1)}}{\partial x} dy_1 + \int_{y_1}^{h_1/2} \frac{\partial \tau_{y_1x}^{(1)}}{\partial y_1} dy_1 = 0, \tag{30}$$

which leads to

$$\tau_{y_1x}^{(1)} = -\frac{1}{h_1}\left[\left(\frac{h_1}{2} - y_1\right) - \frac{3}{h_1}\left(\frac{h_1^2}{4} - y_1^2\right)\right] f_1(x) + \frac{6}{h_1^3}\left(\frac{h_1^2}{4} - y_1^2\right)\int_0^x g_1(\xi) d\xi. \tag{31}$$

In the above, the traction-free BC: $\tau_{y_1x}^{(1)}(h_1/2) = 0$ has been carried out. Furthermore, transverse normal stress $\sigma_{y_1y_1}^{(1)}$ in the cover layer can be calculated by integrating the 2D static equilibrium equation:

$$\frac{\partial \sigma_{y_1y_1}^{(1)}}{\partial y_1} + \frac{\partial \tau_{xy_1}^{(1)}}{\partial x} = 0, \tag{32}$$

with respect to $y_1$ from an arbitrary location $y$ to the top surface at $y_1 = h_1/2$ as

$$\int_{y_1}^{h_1/2} \frac{\partial \sigma_{y_1y_1}^{(1)}}{\partial y_1} dy_1 + \int_{y_1}^{h_1/2} \frac{\partial \tau_{xy_1}^{(1)}}{\partial x} dy_1 = 0, \tag{33}$$

which yields

$$\begin{aligned}\sigma_{y_1y_1}^{(1)} = &-\frac{1}{h_1}\left\{\frac{h_1}{2}\left(\frac{h_1}{2} - y_1\right) - \frac{1}{2}\left(\frac{h_1^2}{4} - y_1^2\right)\right.\\ &\left. - \frac{3}{h_1}\left[\frac{h_1^2}{4}\left(\frac{h_1}{2} - y_1\right) - \frac{1}{3}\left(\frac{h_1^3}{8} - y_1^3\right)\right]\right\} f_1'(x)\\ &+ \frac{6}{h_1^3}\left[\frac{h_1^2}{4}\left(\frac{h_1}{2} - y_1\right) - \frac{1}{3}\left(\frac{h_1^3}{8} - y_1^3\right)\right] g_1(x).\end{aligned} \tag{34}$$

*2.3.2. Planar stresses in the lower adherends*

The stress components in the slender substrate layers can be obtained similarly. The axial normal stress can be approximated to follow the flexural stress formula of classic *Euler–Bernoulli* beams:

$$\begin{aligned}\sigma_{xx}^{(2)} = \frac{S_2}{bh_2} - \frac{M_2 y_2}{I_2} = \frac{1}{h_2}\int_0^x f_2(\xi) d\xi\\ - \frac{12 y_2}{h_2^3}\left[\int_0^x \int_0^\xi g_2(\varsigma) d\varsigma d\xi - \frac{h_2}{2}\int_0^x f_2(\xi) d\xi\right].\end{aligned} \tag{35}$$

Shear stress $\tau_{y_2x}^{(2)}$ can be determined via integrating the 2D static equilibrium equation:

$$\frac{\partial \sigma_{xx}^{(2)}}{\partial x} + \frac{\partial \tau_{y_2x}^{(2)}}{\partial y_2} = 0, \tag{36}$$

with respect to $y_2$ from the bottom surface $y_2 = -h_2/2$ to an arbitrary location $y_2$ of the substrate layer:

$$\int_{-h_2/2}^{y_2} \frac{\partial \sigma_{xx}^{(2)}}{\partial x} dy_2 + \int_{-h_2/2}^{y_2} \frac{\partial \tau_{y_2x}^{(2)}}{\partial y_2} dy_2 = 0, \tag{37}$$

which leads to

$$\begin{aligned}\tau_{y_2x}^{(2)} = &-\frac{1}{h_2}\left[\left(y_2 + \frac{h_2}{2}\right) + \frac{3}{h_2}\left(y_2^2 - \frac{h_2^2}{4}\right) f_2(x)\right.\\ &\left. + \frac{6}{h_2^3}\left(y_2^2 - \frac{h_2^2}{4}\right)\right]\int_0^x g_2(\xi) d\xi.\end{aligned} \tag{38}$$

In the above, the stress-free BC: $\tau_{y_2x}^{(2)}(-h_2/2) = 0$ has been used. Furthermore, normal stress $\sigma_{y_2y_2}^{(2)}$ in the substrate layer can be determined by integrating the 2D equilibrium equation:

$$\frac{\partial \sigma_{y_2y_2}^{(2)}}{\partial y_2} + \frac{\partial \tau_{xy_2}^{(2)}}{\partial x} = 0, \tag{39}$$

with respect to $y_2$ from the bottom surface at $y_2 = -h_2/2$ to an arbitrary location $y_2$:

$$\int_{-h_2/2}^{y_2} \frac{\partial \sigma_{y_2y_2}^{(2)}}{\partial y_2} dy_2 + \int_{-h_2/2}^{y_2} \frac{\partial \tau_{xy_2}^{(2)}}{\partial x} dy_2 = 0, \tag{40}$$

which further reduces to

$$\begin{aligned}\sigma_{y_2y_2}^{(2)} = &\left\{\frac{1}{h_2}\left[\frac{1}{2}\left(y_2^2 - \frac{h_2^2}{4}\right) + \frac{h_2}{2}\left(y_2 + \frac{h_2}{2}\right)\right]\right.\\ &\left. + \frac{3}{h_2^2}\left[\frac{1}{3}\left(y_2^3 + \frac{h_2^3}{8}\right) - \frac{h_2^2}{4}\left(y_2 + \frac{h_2}{2}\right)\right]\right\} f_2'(x)\\ &- \frac{6}{h_2^3}\left[\frac{1}{3}\left(y_2^3 + \frac{h_2^3}{8}\right) - \frac{h_2^2}{4}\left(y_2 + \frac{h_2}{2}\right)\right] g_2(x).\end{aligned} \tag{41}$$

In the above, traction-free BC: $\sigma_{y_2y_2}^{(2)}(-h_2/2) = 0$ has been adopted.

*2.3.3. Planar stresses in the adhesive layer*

The stress components in the adhesive layer can also be derived by the same token. Again, the axial normal stress can be approximated according to the flexural stress formula of classic *Euler–Bernoulli* beams aforementioned:

$$\begin{aligned}\sigma_{xx}^{(0)} = &\frac{S_0}{bh_0} - \frac{M_0 y_0}{I_0}\\ = &\frac{1}{h_0}\int_0^x [f_1(\xi) - f_2(\xi)] d\xi\\ &- \frac{12 y_0}{h_0^3}\left\{\int_0^x \int_0^\xi [g_1(\varsigma) - g_2(\varsigma)] d\varsigma d\xi - \frac{h_0}{2}\int_0^x [f_1(\xi) + f_2(\xi)] d\xi\right\}.\end{aligned} \tag{42}$$

Shear stress $\tau_{y_0x}^{(0)}$ can be determined via integrating the 2D static equilibrium equation:

$$\frac{\partial \sigma_{xx}^{(0)}}{\partial x} + \frac{\partial \tau_{y_0x}^{(0)}}{\partial y_0} = 0, \tag{43}$$

with respect to $y_0$ from the lower interface $y_0 = -h_0/2$ to an arbitrary location $y_0$ of the adhesive layer:

$$\int_{-h_0/2}^{y_0} \frac{\partial \sigma_{xx}^{(0)}}{\partial x} dy_0 + \int_{-h_0/2}^{y_0} \frac{\partial \tau_{y_0x}^{(0)}}{\partial y_0} dy_0 = 0, \tag{44}$$

which leads to

$$\begin{aligned}\tau_{y_0x}^{(0)} = &-f_2(x) - \frac{1}{h_0}\left(y_0 + \frac{h_0}{2}\right)[f_1(x) - f_2(x)] - \frac{3}{h_0^2}\left(y_0^2 - \frac{h_0^2}{4}\right)[f_1(x) + f_2(x)]\\ &+ \frac{6}{h_0^3}\left(y_0^2 - \frac{h_0^2}{4}\right)\int_0^x [g_1(\xi) - g_2(\xi)] d\xi.\end{aligned} \tag{45}$$

In the above, the stress-continuity BC: $\tau_{y_0x}^{(0)}(-h_0/2) = -f_2(x)$ has been evoked. Furthermore, normal stress $\sigma_{y_0y_0}^{(0)}$ in the adhesive layer can be determined by integrating the 2D equilibrium equation:

$$\frac{\partial \sigma_{y_0y_0}^{(0)}}{\partial y_0} + \frac{\partial \tau_{xy_0}^{(0)}}{\partial x} = 0, \tag{46}$$

with respect to $y_0$ from the bottom surface at $y_0 = -h_0/2$ to an arbitrary location $y_0$:

$$\int_{-h_0/2}^{y_0} \frac{\partial \sigma_{y_0 y_0}^{(0)}}{\partial y_0} dy_0 + \int_{-h_0/2}^{y_0} \frac{\partial \tau_{xy_0}^{(0)}}{\partial x} dy_0 = 0, \tag{47}$$

which can be further reduced to

$$\begin{aligned}\sigma_{y_0 y_0}^{(0)} = {} & g_2(x) + \left(y_0 + \frac{h_0}{2}\right) f_2'(x) \\ & + \frac{1}{h_0}\left[\frac{1}{2}\left(y_0^2 - \frac{h_0^2}{4}\right) + \frac{h_0}{2}\left(y_0 + \frac{h_0}{2}\right)\right][f_1'(x) - f_2'(x)] \\ & + \frac{3}{h_0^2}\left[\frac{1}{3}\left(y_0^3 + \frac{h_0^3}{8}\right) - \frac{h_0^2}{4}\left(y_0 + \frac{h_0}{2}\right)\right][f_1'(x) + f_2'(x)] \\ & - \frac{6}{h_0^3}\left[\frac{1}{3}\left(y_0^3 + \frac{h_0^3}{8}\right) - \frac{h_0^2}{4}\left(y_0 + \frac{h_0}{2}\right)\right][g_1(x) - g_2(x)].\end{aligned} \tag{48}$$

In the above, stress-continuity BC: $\sigma_{y_0 y_0}^{(0)}(-h_0/2) = g_2(x)$ has been adopted. If setting $y_0 = h_0/2$, expressions (45) and (48) can be consistently reduced to $\tau_{y_0 x}^{(0)}(h_0/2) = -f_1(x)$ and $\sigma_{y_0 y_0}^{(0)}(h_0/2) = g_1(x)$, where the minus sign prior to $f(x)$ is due to the sign conversion of stress components in elasticity.

From the above derivation, it can be concluded that with the approximation of axial normal stress varying linearly across the cover, substrate and adhesive layers, the corresponding statically compatible shear and transverse normal stresses vary piecewise parabolically and cubically across these layers, respectively. More importantly, such a stress field satisfies all the traction BCs at the ends of the adherend and adhesive layers, and the stress continuity across the interfaces between the adherend and adhesive is also fulfilled.

### 2.4. Governing equations of interfacial stress functions and solution

With the above stress components in the ABJ, the strain energy of the right half-joint ($0 \leqslant x \leqslant L$) is

$$\begin{aligned}U = {} & b\int_0^L \int_{-h_1/2}^{h_1/2} \left\{\frac{1}{2}\left[\sigma_{xx}^{(1)}\varepsilon_{xx}^{(1)} + \sigma_{yy}^{(1)}\varepsilon_{yy}^{(1)}\right] + \frac{1+\upsilon_1}{E_1}\left[\tau_{xy_1}^{(1)}\right]^2\right\} dx dy_1 \\ & + b\int_0^L \int_{-h_2/2}^{h_2/2} \left\{\frac{1}{2}\left[\sigma_{xx}^{(2)}\varepsilon_{xx}^{(2)} + \sigma_{yy}^{(2)}\varepsilon_{yy}^{(2)}\right] + \frac{1+\upsilon_2}{E_2}\left[\tau_{xy_2}^{(2)}\right]^2\right\} dx dy_2 \\ & + b\int_0^L \int_{-h_0/2}^{h_0/2} \left\{\frac{1}{2}\left[\sigma_{xx}^{(0)}\varepsilon_{xx}^{(0)} + \sigma_{yy}^{(0)}\varepsilon_{yy}^{(0)}\right] + \frac{1+\upsilon_0}{E_0}\left[\tau_{xy_0}^{(0)}\right]^2\right\} dx dy_0.\end{aligned} \tag{49}$$

In the above, $\varepsilon_{xx}^{(i)}$ and $\varepsilon_{yy}^{(i)}$ ($i = 0,1,2$) are respectively the axial and transverse normal strains of the adhesive layer, upper and lower adherends, which are defined according to the generalized Hooke's law of isotropic, linearly thermoelastic solids (in the *plane-stress* state):

$$\varepsilon_{xx}^{(i)} = \frac{1}{E_i}\sigma_{xx}^{(i)} - \frac{\upsilon_i}{E_i}\sigma_{yy}^{(i)} + \alpha_i \Delta T, \tag{50}$$

$$\varepsilon_{yy}^{(i)} = \frac{1}{E_i}\sigma_{yy}^{(i)} - \frac{\upsilon_i}{E_i}\sigma_{xx}^{(i)} + \alpha_i \Delta T, \tag{51}$$

where $\alpha_i (i = 0,1,2)$ are coefficients of thermal expansion of the adhesive layer, upper and lower adherends, respectively, and $\Delta T$ is the uniform temperature change of the joint from the reference temperature of free thermomechanical stress state. In the sense of mathematics, strain energy (49) is an energy functional with respect to the four unknown interfacial stress-functions $f_i (i = 1,2)$ and $g_i (i = 1,2)$ adopted above. According to theorem of minimum complimentary strain energy of an elastic body, the strain energy of the joint reaches a stationary point at static equilibrium of the joint, which corresponds to the necessary condition in terms of variation of the strain energy (49) with respect to the four unknown stress functions

$$\delta U = 0, \tag{52}$$

i.e.,

$$\begin{aligned}\delta U = {} & b\int_0^L \int_{-h_1/2}^{h_1/2} \left\{\frac{1}{2}\left[\sigma_{xx}^{(1)}\delta\varepsilon_{xx}^{(1)} + \delta\sigma_{xx}^{(1)}\varepsilon_{xx}^{(1)} + \sigma_{yy}^{(1)}\delta\varepsilon_{yy}^{(1)} + \delta\sigma_{yy}^{(1)}\varepsilon_{yy}^{(1)}\right] \right. \\ & \left. + \frac{2(1+\upsilon_1)}{E_1}\tau_{xy_1}^{(1)}\delta\tau_{xy_1}^{(1)}\right\} dx dy_1 \\ & + b\int_0^L \int_{-h_2/2}^{h_2/2} \left\{\frac{1}{2}\left[\sigma_{xx}^{(2)}\delta\varepsilon_{xx}^{(2)} + \delta\sigma_{xx}^{(2)}\varepsilon_{xx}^{(2)} + \sigma_{yy}^{(2)}\delta\varepsilon_{yy}^{(2)} + \delta\sigma_{yy}^{(2)}\varepsilon_{yy}^{(2)}\right] \right. \\ & \left. + \frac{2(1+\upsilon_2)}{E_2}\tau_{xy_2}^{(2)}\delta\tau_{xy_2}^{(2)}\right\} dx dy_2 \\ & + b\int_0^L \int_{-h_0/2}^{h_0/2} \left\{\frac{1}{2}\left[\sigma_{xx}^{(0)}\delta\varepsilon_{xx}^{(0)} + \delta\sigma_{xx}^{(0)}\varepsilon_{xx}^{(0)} + \sigma_{yy}^{(0)}\delta\varepsilon_{yy}^{(0)} + \delta\sigma_{yy}^{(0)}\varepsilon_{yy}^{(0)}\right] \right. \\ & \left. + \frac{2(1+\upsilon_0)}{E_0}\tau_{xy_0}^{(0)}\delta\tau_{xy_0}^{(0)}\right\} dx dy_0.\end{aligned} \tag{53}$$

where $\delta$ is the mathematical varational operator with respect to either $f_i (i = 1,2)$ or $g_i (i = 1,2)$.

By substituting the stress expressions (28), (31), (34), (35), (38), (41), (42), (45), (48), and normal strains (50) and (51) into (53) and evoking the variational operation and several mathematical simplifications, it yields the interfacial stress functions $f_1$, $f_2$, $g_1$, and $g_2$ to satisfy a system of four coupled 4th-order ODEs of constant coefficients:

$$[A]\left\{\Phi^{(IV)}\right\} + [B]\{\Phi''\} + [C]\{\Phi\} + \{D\} = \{0\}. \tag{54}$$

In the above, $\{\Phi\}_{4\times 1}$ is a dimensionless interfacial stress function vector defined as

$$\{\Phi\} = \{F_1(\xi), G_1(\xi), F_2(\xi), G_2(\xi)\}^T, \tag{55}$$

$$F_1(\xi) = F_1(x/h_2) = -\frac{1}{p_0 h_2}\int_0^x f_1(\zeta) d\zeta, \tag{56a}$$

$$F_2(\xi) = F_2(x/h_2) = -\frac{1}{p_0 h_2}\int_0^x f_2(\zeta) d\zeta, \tag{56b}$$

$$G_1(\xi) = G_1(x/h_2) = \frac{1}{p_0 h_2^2}\int_0^x \int_0^\zeta g_1(\eta) d\eta d\zeta, \tag{56c}$$

$$G_2(\xi) = G_2(x/h_2) = \frac{1}{p_0 h_2^2}\int_0^x \int_0^\zeta g_2(\eta) d\eta d\zeta. \tag{56d}$$

$[A]$, $[B]$ and $[C]$ are three $4 \times 4$ real-valued symmetric coefficient matrices, which are related to the elastic properties and layer thickness of the ABJ as

$$[A] = \begin{bmatrix} \frac{1}{105}\left(h_{02}^3 e_{20} + h_{12}^3 e_{21}\right) & \frac{11}{210}\left(h_{02}^2 e_{20} - h_{12}^2 e_{21}\right) & -\frac{1}{140}h_{02}^3 e_{20} & \frac{13}{420}h_{02}^2 e_{20} \\ & \frac{13}{35}(h_{02}e_{20} + h_{12}e_{21}) & -\frac{13}{420}h_{02}^2 e_{20} & \frac{9}{70}h_{02}e_{20} \\ & & \frac{1}{105}(1 + h_{02}^3 e_{20}) & \frac{11}{210}\left(1 - h_{02}^2 e_{20}\right) \\ \text{Sys} & & & \frac{13}{35}(1 + h_{02}e_{20}) \end{bmatrix}, \tag{57a}$$

$$[B] = \begin{bmatrix} -\frac{4}{15}(h_{02}e_{20} + h_{12}e_{21}) & \frac{1}{5}(-e_{20} + e_{21}) + \upsilon_0 e_{20} - \upsilon_1 e_{21} & \frac{1}{15}h_{02}e_{20} & \frac{1}{5}e_{20} \\ & -\frac{12}{5}\left(h_{02}^{-1}e_{20} + h_{12}^{-1}e_{21}\right) & -\frac{1}{5}e_{20} & \frac{12}{5}h_{02}^{-1}e_{20} \\ & & -\frac{4}{15}(1 + h_{02}e_{20}) & -\frac{1}{5}(1 - e_{20}) - \upsilon_0 e_{20} + \upsilon_2 \\ \text{Sys} & & & -\frac{12}{5}\left(1 + h_{02}^{-1}e_{20}\right) \end{bmatrix} \tag{57b}$$

and

$$[C]=\begin{bmatrix} 4\left(h_{02}^{-1}e_{20}+h_{12}^{-1}e_{21}\right) & 6\left(h_{02}^{-2}e_{20}-h_{12}^{-2}e_{21}\right) & 2h_{02}^{-1}e_{20} & -6h_{02}^{-2}e_{20} \\ & 12\left(h_{02}^{-3}e_{20}+h_{12}^{-3}e_{21}\right) & 6h_{02}^{-2}e_{20} & -12h_{02}^{-3}e_{20} \\ & & 4(1+h_{02}^{-1}e_{20}) & 6\left(1-h_{02}^{-2}e_{20}\right) \\ \text{Sys} & & & 12\left(1+h_{02}^{-3}e_{20}\right) \end{bmatrix}, \tag{57c}$$

where

$$h_{02}=h_0/h_2, \quad h_{12}=h_1/h_2, \quad e_{20}=E_2/E_0, \quad e_{21}=E_2/E_1. \tag{58}$$

$\{D\}_{4\times1}$ is a dimensionless $4\times1$ mechanical or thermomechanical load vector:

$$\{D\}=\{D_1,D_2,D_3,D_4\}^T, \tag{59}$$

in which

$$D_1=h_{12}^{-1}\left[1+3(1+2h_{02}+h_{12})h_{12}^{-2}\right]e_{21}+\frac{1}{2}(\alpha_1-\alpha_0)\Delta T E_2/p_0, \tag{60a}$$

$$D_2=-6(1+2h_{02}+h_{12})h_{12}^{-3}e_{21}, \tag{60b}$$

$$D_3=-\frac{1}{2}(\alpha_2-\alpha_0)\Delta T E_2/p_0, \tag{60c}$$

$$D_4=0. \tag{60d}$$

In the above, when the thermomechanical stress state of the joint due to a pure temperature change is considered, the stress $p_0$ adopted in (60a) and (60c) is understood as a stress reference for the purpose of dimensionless formulation. In addition, these governing equations can be conveniently extended to the cases of *plane strain* state by replacing $E_i$ with $E_i/(1-\upsilon_i^2)$, $\upsilon_i$ with $\upsilon_i/(1-\upsilon_i)$, and $\alpha_i$ with $(1+\upsilon_i)\alpha_i$, where $i=0$, 1, and 2, as mentioned above.

Solution to (54) can be determined by superimposing the general solution $\{\Psi\}$ of the corresponding set of homogenous ODEs to a particular solution $\{\Phi_0\}$ (Wu and Jenson, 2011):

$$\{\Phi\}=\{\Psi\}+\{\Phi_0\}, \tag{61}$$

$$[A]\left\{\Psi^{(IV)}\right\}+[B]\{\Psi''\}+[C]\{\Psi\}=\{0\}, \tag{62}$$

$$\{\Phi_0\}=-[C]^{-1}\{\mathrm{D}\}. \tag{63}$$

To solve the system of homogenous ODEs (62), assume the general solution $\{\Psi\}$ carrying the form:

$$\{\Psi\}=\{\Psi_0\}\exp(\lambda\xi), \tag{64}$$

where $\lambda$ and $\{\Psi_0\}$ are respectively the eigenvalue and eigenvector of the characteristic equation corresponding to homogenous ODEs (62):

$$\lambda^4[A]\{\Psi_0\}+\lambda^2[B]\{\Psi_0\}+[C]\{\Psi_0\}=\{0\}. \tag{65}$$

Eq. (65) is a generalized eigenvalue problem, which can be converted into a standard eigenvalue problem by introducing

$$\{\Psi_1\}=\lambda^2\{\Psi_0\}. \tag{66}$$

Thus, the eigenvalue problem (65) is converted into a standard form:

$$\begin{bmatrix} \mathrm{I} & 0 \\ 0 & \mathrm{A} \end{bmatrix}\begin{Bmatrix} \Psi_0 \\ \Psi_1 \end{Bmatrix}=-\lambda^{-2}\begin{bmatrix} 0 & -I \\ \mathrm{C} & \mathrm{B} \end{bmatrix}\begin{Bmatrix} \Psi_0 \\ \Psi_1 \end{Bmatrix}, \tag{67}$$

where $I$ is a $8\times8$ identity. This eigenvalue problem can be solved efficiently by using well developed robust numerical algorithms available in the literature (e.g., the eig() function provided by Matlab™, etc.). As a result, the final expression of the general solution (61) is

$$\{\Phi\}=\sum_{k=1}^{8}\left[c_k\{\Psi_0^k\}\exp(\lambda_k\xi)+d_k\{\Psi_0^k\}\exp(-\lambda_k\xi)\right]+\{\Phi_0\}, \tag{68}$$

where $\{\Psi_0^k\}$ ($k=1,2,\ldots,8$) are eigenvectors (the first 4 elements of each column) attached to eigenvalues $\lambda_k$($k=1,2,\ldots,8$), respectively, and $c_k$ and $d_k$($k=1,2,\ldots,8$) are the real or complex coefficients to be determined in satisfying the traction BCs (12a), (12b), and (13a)-(13r). Herein, only 16 BCs are linearly independent that can be extracted from these traction BCs for determining the unknown coefficients $c_k$ and $d_k$($k=1,2,\ldots,8$):

$$F_1(0)=0, \tag{69a}$$

$$F_1(L/h_2)=-1, \tag{69b}$$

$$F_1'(0)=0, \tag{69c}$$

$$F_1'(L/h_2)=0, \tag{69d}$$

$$G_1(0)=0, \tag{69e}$$

$$G_1(L/h_2)=1/2+h_{02}, \tag{69f}$$

$$G_1'(0)=0, \tag{69g}$$

$$G_1'(L/h_2)=0. \tag{69h}$$

$$F_2(0)=0, \tag{69i}$$

$$F_2(L/h_2)=-1, \tag{69j}$$

$$F_2'(0)=0, \tag{69k}$$

$$F_2'(L/h_2)=0, \tag{69l}$$

$$G_2(0)=0, \tag{69m}$$

$$G_2(L/h_2)=1/2, \tag{69n}$$

$$G_2'(0)=0, \tag{69o}$$

$$G_2'(L/h_2)=0. \tag{69p}$$

Consequently, plugging (61) and (68) into (69a)-(69p) yields a system of 16 simultaneous linear algebraic equations:

$$\sum_{k=1}^{8}c_k\Psi_0^{k,1}+\sum_{k=1}^{8}d_k\Psi_0^{k,1}=-\Phi_0^{(1)}, \tag{70a}$$

$$\sum_{k=1}^{8}c_k\Psi_0^{k,1}\exp(\lambda_kL/h_2)+\sum_{k=1}^{8}d_k\Psi_0^{k,1}\exp(-\lambda_kL/h_2)=-\left[1+\Phi_0^{(1)}\right], \tag{70b}$$

$$\sum_{k=1}^{8}c_k\lambda_k\Psi_0^{k,1}-\sum_{k=1}^{8}d_k\lambda_k\Psi_0^{k,1}=0, \tag{70c}$$

$$\sum_{k=1}^{8}c_k\lambda_k\Psi_0^{k,1}\exp(\lambda_kL/h_2)-\sum_{k=1}^{8}d_k\lambda_k\Psi_0^{k,1}\exp(-\lambda_kL/h_2)=0, \tag{70d}$$

$$\sum_{k=1}^{8}c_k\Psi_0^{k,2}+\sum_{k=1}^{8}d_k\Psi_0^{k,2}=-\Phi_0^{(2)}, \tag{70e}$$

$$\sum_{k=1}^{8} c_k \Psi_0^{k,2} \exp(\lambda_k L/h_2) + \sum_{k=1}^{8} d_k \Psi_0^{k,2} \exp(-\lambda_k L/h_2) = 1/2 + h_{02} - \Phi_0^{(2)}, \tag{70f}$$

$$\sum_{k=1}^{8} c_k \lambda_k \Psi_0^{k,2} - \sum_{k=1}^{8} d_k \lambda_k \Psi_0^{k,2} = 0, \tag{70g}$$

$$\sum_{k=1}^{8} c_k \lambda_k \Psi_0^{k,2} \exp(\lambda_k L/h_2) - \sum_{k=1}^{8} d_k \lambda_k \Psi_0^{k,2} \exp(-\lambda_k L/h_2) = 0. \tag{70h}$$

$$\sum_{k=1}^{8} c_k \Psi_0^{k,3} + \sum_{k=1}^{8} d_k \Psi_0^{k,3} = -\Phi_0^{(3)}, \tag{70i}$$

$$\sum_{k=1}^{8} c_k \Psi_0^{k,3} \exp(\lambda_k L/h_2) + \sum_{k=1}^{8} d_k \Psi_0^{k,3} \exp(-\lambda_k L/h_2) = -\left[1 + \Phi_0^{(3)}\right], \tag{70j}$$

$$\sum_{k=1}^{8} c_k \lambda_k \Psi_0^{k,3} - \sum_{k=1}^{8} d_k \lambda_k \Psi_0^{k,3} = 0, \tag{70k}$$

$$\sum_{k=1}^{8} c_k \lambda_k \Psi_0^{k,3} \exp(\lambda_k L/h_2) - \sum_{k=1}^{8} d_k \lambda_k \Psi_0^{k,3} \exp(-\lambda_k L/h_2) = 0, \tag{70l}$$

$$\sum_{k=1}^{8} c_k \Psi_0^{k,4} + \sum_{k=1}^{8} d_k \Psi_0^{k,4} = -\Phi_0^{(4)}, \tag{70m}$$

$$\sum_{k=1}^{8} c_k \Psi_0^{k,4} \exp(\lambda_k L/h_2) + \sum_{k=1}^{8} d_k \Psi_0^{k,4} \exp(-\lambda_k L/h_2) = 1/2 - \Phi_0^{(4)}, \tag{70n}$$

$$\sum_{k=1}^{8} c_k \lambda_k \Psi_0^{k,4} - \sum_{k=1}^{8} d_k \lambda_k \Psi_0^{k,4} = 0, \tag{70o}$$

$$\sum_{k=1}^{8} c_k \lambda_k \Psi_0^{k,4} \exp(\lambda_k L/h_2) - \sum_{k=1}^{8} d_k \lambda_k \Psi_0^{k,4} \exp(-\lambda_k L/h_2) = 0. \tag{70p}$$

In the above, $\Psi_0^{k,1}$, $\Psi_0^{k,2}$, $\Psi_0^{k,3}$, and $\Psi_0^{k,4}$ ($k = 1,2,\ldots,8$) are respectively the 1st–4th elements of the $k$-th eigenvector, and $\Phi_0^{(1)}$, $\Phi_0^{(2)}$, $\Phi_0^{(3)}$, and $\Phi_0^{(4)}$ are the 1st–4th elements of the particular solution vector $\{\Phi_0\}$. Moreover, in the case of thermomechanical stress analysis of the joint due to a pure temperature change, the right terms of (69b), (69f), (69j) and (69n) should be specified as zeros, which further influence the right terms of (70b), (70f), (70j) and (70n) accordingly. Once $c_k (k = 1,2,\ldots,8)$ and $d_k (k = 1,2,\ldots,8)$ are determined by solving the above set of linear algebraic equations (70a)-(70p) numerically, relations (56a)-(56d) and (68) finalize the four interfacial stress functions $f_i$ and $g_i (i = 1,2)$ as

$$f_1(x)/p_0 = -\sum_{k=1}^{8} c_k \Psi_0^{k,1} \lambda_k \exp(\lambda_k x/h_2) + \sum_{k=1}^{8} d_k \Psi_0^{k,1} \lambda_k \exp(-\lambda_k x/h_2), \tag{71a}$$

$$g_1(x)/p_0 = \sum_{k=1}^{8} c_k \Psi_0^{k,2} \lambda_k^2 \exp(\lambda_k x/h_2) + \sum_{k=1}^{8} d_k \Psi_0^{k,2} \lambda_k^2 \exp(-\lambda_k x/h_2). \tag{71b}$$

$$f_2(x)/p_0 = -\sum_{k=1}^{8} c_k \Psi_0^{k,3} \lambda_k \exp(\lambda_k x/h_2) + \sum_{k=1}^{8} d_k \Psi_0^{k,3} \lambda_k \exp(-\lambda_k x/h_2), \tag{71c}$$

$$g_2(x)/p_0 = \sum_{k=1}^{8} c_k \Psi_0^{k,4} \lambda_k^2 \exp(\lambda_k x/h_2) + \sum_{k=1}^{8} d_k \Psi_0^{k,2} \lambda_k^2 \times \exp(-\lambda_k x/h_2). \tag{71d}$$

Consequently, with the four interfacial stress functions $f_i$ and $g_i (i = 1,2)$ given in (71a)-(71d), all the planar stresses in the adherends and adhesive layer of the ABJ can be determined according to the expressions formulated in Section 2.3. It needs to be mentioned that except the expressions of the stress resultants and BCs of the adhesively single-sided strap joint, all the derivations above are actually independent of the specific configuration of the joint. Thus, the governing Eq. (54) and system matrices (57a)-(57c) are applicable to other statically equivalent ABJs such as adhesively bonded single-lap joints.

## 3. Model validation, parameter studies and discussions

### 3.1. Interfacial stresses in adhesively single-sided strap joints due to mechanical loads

Let us first consider the interfacial shear and normal stresses at the upper and lower surfaces of the adhesive layer of an adhesively single-sided strip joint subjected to uniform axial tension in the plane-stress state. Commercial FEM software package (ANSYS™) is used to validate the interfacial stresses predicted by the current semi-analytic method. When ignoring the adhesive layer, i.e., a bonded single-sided strap joint, our recent study (Wu and Jenson 2011) has showed that the stress-function variational method based on two interfacial stress functions can accurately predict the interfacial shear and normal stresses, which have been validated by our FEM simulation and other recently developed models in the literature (e.g., Yousefsani and Tahani, 2013a,b). In the present case as shown in Fig. 2, the ABJ is assumed to be made of a steel cover layer ($E_1 = 210$ GPa, $\upsilon_1 = 0.293$) and two identical aluminum substrate layers ($E_2 = 70$ GPa, $\upsilon_2 = 0.345$), which are adhesively bonded together with an epoxy-type adhesive layer ($E_0 = 10$ GPa, $\upsilon_0 = 0.40$). The adherends and adhesive layer have the same width; other geometries of the joint are: $h_1 = 2.0$ mm (steel), $h_2 = 2.0$ mm (aluminum), $h_0 = 0.2$ mm (adhesive), and $L = 20$ mm (see Fig. 2). A uniform tensile traction with the unit magnitude $p_0 = 1$ MPa is applied to the substrate layers. During the stress analysis based on ANSYS™, four-node elements (PLANE182) and mapped uniform quadrilateral meshes are utilized. In an attempt to track the trend of the singular stresses at free edges of the adherends, two refined mesh sizes (i.e., quadrilateral elements with the dimensions of $0.05 \times 0.05$ mm and $0.01 \times 0.01$ mm, respectively) are employed at the two free-edge corners of the adherends. Variations of the interfacial shear and normal stresses at the upper and lower adhesive surfaces with the distance from the mid-span to the right adherend end are plotted in Fig. 4(a) and (*b*). Due to the existence of the bending moment resultant at the mid-span of the joint (see Fig. 1), both the high interfacial shear and normal stresses are observed at the mid-span free-edge. This high normal (peeling) stress is responsible mainly for the debonding failure of the ABJ, while the high shear stress further enhances the effective failure stress, e.g., *von Mises stress*, near the free edges of the adherend at the mid-span. Furthermore, stress comparisons in Fig. 4(a) and (*b*) can conclude that the present model can accurately predict both the interfacial shear and normal stresses of ABJs, especially for the interfacial normal stresses. Also, the predicted interfacial shear stresses exactly satisfy the shear-free condition at the free edges.

In addition, as shown in Fig. 4, though both the interfacial normal and shear stresses at the upper and lower surfaces of the adhesive layer carry the very similar varying trends along the interfaces, the variations of these stresses from the upper to the lower surface

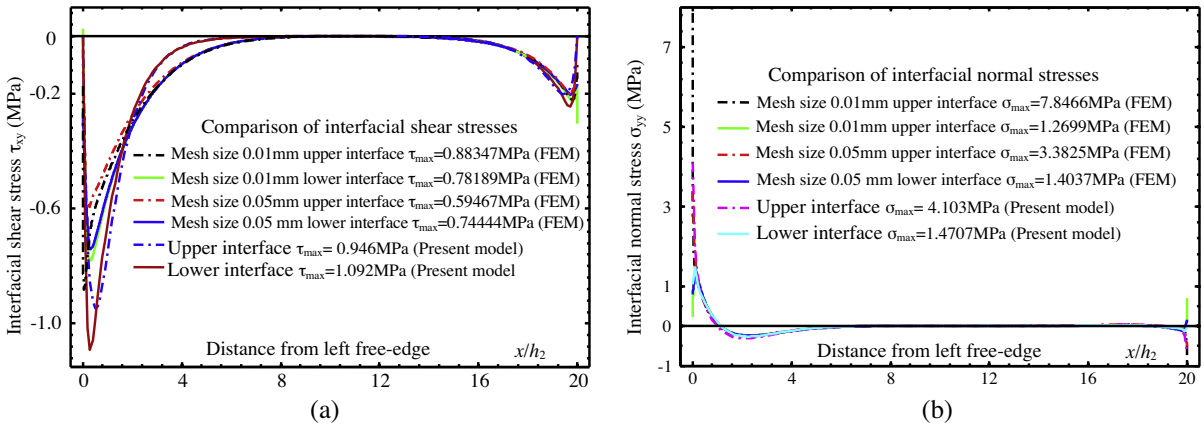


**Fig. 4.** Validation of the stress-function variational method for prediction of the interfacial shear and normal stresses at the upper and lower surfaces of the adhesive layer (*plane-stress*) by finite element analysis (ANSYS™): (*a*) interfacial shear stress $\tau$ and (*b*) interfacial normal stress $\sigma$. Material properties: upper adherend: aluminum with $E_1 = 70$ GPa, $\upsilon_1 = 0.345$ and $h_1 = 2.0$ mm; lower adherends: Steel with $E_2 = 210$ GPa, $\upsilon_2 = 0.293$ and $h_2 = 2.0$ mm; epoxy-type adhesive: $E_0 = 10$ GPa, $\upsilon_0 = 0.4$, $h_0 = 0.2$ mm.

of the adhesive layer could be noticeably large near the free edges, especially the interfacial normal stress. Such an observation seems to conflict with the common assumptions adopted in many ABJ models in the literature such that *the shear and normal stresses do not change significantly across the adhesive layer due to the thin thickness of the adhesive layer*. To interpret such an important observation, let us consider the static equilibrium of a segmental element (with the length $\Delta x$) of the adhesive layer near the free-edge as illustrated in Fig. 5, the static equilibrium equation along $y$-direction reads

$$\left(\bar{\sigma}_{yy}^{\frac{h_0}{2}} - \bar{\sigma}_{yy}^{-\frac{h_0}{2}}\right)\Delta x - \tau_{xy} h_0 = 0, \tag{72}$$

where $\bar{\sigma}_{yy}^{\frac{h_0}{2}}$ and $\bar{\sigma}_{yy}^{-\frac{h_0}{2}}$ are the average normal stresses at the upper and lower adhesive surfaces over the layer length $\Delta x$, respectively. Thus, the difference of the average normal stress across the adhesive layer can be estimated from (72) as

$$\Delta\sigma_{yy} = \bar{\sigma}_{yy}^{\frac{h_0}{2}} - \bar{\sigma}_{yy}^{-\frac{h_0}{2}} = \tau_{xy}\frac{h_0}{\Delta x}. \tag{73}$$

Near the free edges of the adherends, the shear stress becomes very large. When $\Delta x$ is selected to be comparable to or smaller than the thickness of the adhesive layer $h_0$, $\Delta\sigma_{yy}$ could become large, even significant depending on the interfacial shear stress. In addition, such a stress difference decays rapidly with the increasing distance from the free edge. Therefore, in the classic ABJ models, the assumption of approximately constant normal and shear stresses across the thin adhesive layer is *questionable* at the region very close to the free ends of the adherends.

Furthermore, due to the nature of Williams-type stress singularity (singular wedge stress field) near the free-edges of bonded

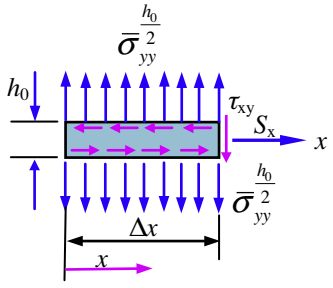


**Fig. 5.** Free-body diagram of a representative adhesive layer segment near the adherend end.

materials, the interfacial stresses predicted by FEA increase rapidly with decreasing mesh size. Like most analytic models available in the literature, the present model is unable to predict such singularity. However, the very good fitting into the interfacial stress trends predicted by FEA validates the present model for stress analysis of ABJs, which can be exploited for scaling analysis, structural design and optimization of ABJs, etc.

### 3.2. Thermomechanical stresses in adhesively bonded thermostats

Thermomechanical stress analysis of an adhesively single-sided strap joint (see Fig. 2) due purely to a uniform temperature change is equivalent to that of an adhesively bonded thermostat. Thermomechanical stress analysis of a bonded biomaterial thermostat (e.g., aluminum–molybdenum) has been extensively studied by a number of investigators such as Suhir (1989), Eischen et al. (1990) and Ru (2002), etc. Our recent work has demonstrated the reliability of stress-function variational method for solving such type of problems (Wu and Jenson, 2011). To demonstrate the present semi-analytic method for determining the thermomechanical stresses in adhesively bonded thermostats, we introduce a thin adhesive layer into the aforementioned aluminum–molybdenum thermostat. In the present symbolic system, the parameters of the thermostat considered in prior studies are: $h_1 = 2.5$ mm, $E_1 = 70$ GPa, $\upsilon_1 = 0.345$, $\alpha_1 = 23.6 \times 10^{-6}/°C$, $h_2 = 2.5$ mm, $E_2 = 325$ GPa, $\upsilon_2 = 0.293$, $\alpha_2 = 4.9 \times 10^{-6}/°C$, $L = 50.8$ mm and $\Delta T = 240$ °C. The properties of the adhesive layer in this study are assumed as $E_0 = 10$ GPa, $\upsilon_0 = 0.40$, and $\alpha_0 = 73.8 \times 10^{-6}/°C$, and two thicknesses of the adhesive layer are sampled: $h_0 = 0.25$ mm and 1.0 mm, respectively. In addition, the adhesively bonded thermostat is assumed in the *plane-strain* state as used in the previous studies.

For the purpose of comparison, Fig. 6(a) and (*b*) show the distributions of thermomechanical shear and normal stresses along the interface of a bimaterial thermostat, respectively, in our recent study based on the stress-function variational method (Wu and Jenson, 2011). These stress predictions are very close to those predicted by Suhir (1989), Eischen et al. (1990) and Ru (2002), etc. Fig. 6(*c*)–(*f*) plot the shear and normal stress variations at the upper and lower surfaces of the adhesive layer at two different thicknesses ($h_0 = 0.25$ mm and 1.0 mm) in the adhesively bonded thermostat based on the present method. In the case of an adhesively bonded thermostat with a relatively thin adhesive layer ($h_0 = 0.25$ mm), both the shear and normal stresses at the upper and lower surfaces of the adhesive layer carry very similar varying

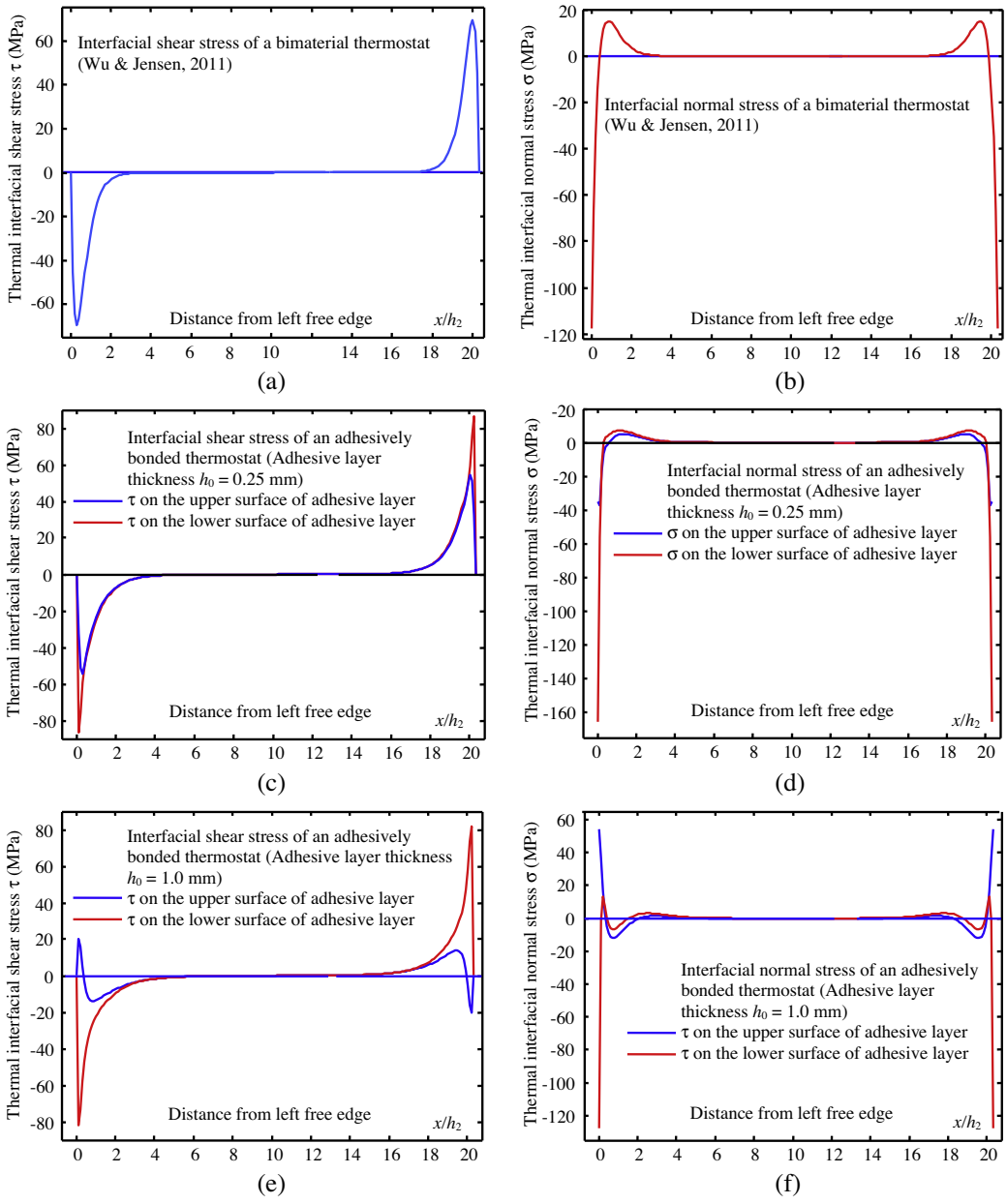


**Fig. 6.** Comparison of thermomechanical interfacial shear and normal stresses between an adhesively bonded aluminum/molybbdenum thermostat and an aluminum/molybbdenum bimaterial thermostat subjected to uniform temperature change ($\Delta T = 240$ °C) (*plane-strain*). Material properties: aluminum: $E_1 = 70$ GPa, $\upsilon_1 = 0.345$, $\alpha_1 = 23.6 \times 10^{-6}$/°C, $h_1 = 2.5$ mm; molybbdenum: $E_2 = 325$ GPa, $\upsilon_2 = 0.293$, $\alpha_2 = 4.9 \times 10^{-6}$/°C, $h_2 = 2.5$ mm; epoxy-type adhesive: $E_0 = 10$ GPa, $\upsilon_0 = 0.4$, $\alpha_0 = 73.8 \times 10^{-6}$/°C; thermostat length: $L = 50.8$ mm.

trends to those of the bimaterial thermoset above (Fig. 6(a) and (*b*)). The peak values of both the shear and normal stresses at the lower surface of the adhesive layer are nearly 40% higher than those of the bimaterial thermostat with the same geometries, material properties, and temperature change. In contrast, at the upper surface of the adhesive layer, the peak values of both the shear and normal stresses are lower than those of the bimaterial thermostat. Specifically, the peak value of shear stress is decreased ~20%, while the peak value of normal stress is decreased around two-thirds. By examining the system, the adhesive layer exhibits a very large thermal expansion compared to either the upper or lower adherend. Such a large thermal expansion in the adhesive interlayer is responsible for the higher interfacial stresses at the lower surface of the adhesive layer, which is constrained by a stiffer adherend. Compared to the stiffer lower adherend, the compliant upper adherend is more pliable to deform under the inconsistent thermal expansion via deflection, corresponding to the lower shear and normal stresses on the upper surface of adhesive layer.

Furthermore, in the case of a thick adhesive layer ($h_0 = 1.0$ mm), both the shear and normal stresses (Fig. 6(e) and (*f*)) at the lower surface of the adhesive layer carry a slight decrease compared to the case of a thinner adhesive layer (Fig. 6(c) and (*d*)). This observation can be understood such that the large thickness and low modulus of the adhesive layer could accommodate relatively large mismatched deformations between the upper and lower adherends due to the inconsistent thermal expansion. In contrast, at the upper surface of the adhesive layer, the directions of both the shear and normal stresses are altered, corresponding to the change of the characteristic deflection of the upper adherend induced by

the varying adhesive layer thickness. In this case, compared to the case of a thinner adhesive layer, the peak value of interfacial shear stress at the upper interface decreases nearly half, while the peak value of interfacial normal stress nearly doubles.

### 3.3. Scaling analysis of interfacial stresses

A compact, efficient computational code is designed to implement the present stress-function variational method for stress analysis of ABJs. This code can be used to examine the dependencies of the interfacial shear and normal stresses upon all the geometrical and material parameters of the ABJs including the layer thickness ratios $h_0/h_2$ and $h_1/h_2$, length ratio $L/h_2$, modulus ratios $E_0/E_2$ and $E_1/E_2$, Poisson's ratios $\upsilon_0$, $\upsilon_1$ and $\upsilon_2$, and coefficients of thermal expansion $\alpha_0$, $\alpha_1$ and $\alpha_2$. In our recent study of single-sided strap joints (Wu and Jenson, 2011), substantial scaling studies have been conducted to examine the effects of adherend thickness ratio $h_1/h_2$, length ratio $L/h_2$ and modulus ratio $E_1/E_2$ on the shear and normal stress variations along the interface. In the following, we are going to examine the effects of the thickness and modulus of the adhesive layer on the interfacial shear and normal stresses. In addition, it needs to be mentioned that the present ABJ model is established within the framework of linear elasticity. Therefore, the stress field in ABJs triggered by combined mechanical loads and temperature change can be treated separately based on method of superposition.

#### 3.3.1. Scaling analysis of interfacial stresses due to mechanical loads

To examine the effects of thickness and modulus of the adhesive layer on the interfacial shear and normal stresses in the present ABJ, the adherend length and modulus ratios are fixed as $L/h_2 = 5$ and $E_1/E_2 = 3$, and Poisson's ratios of the upper and lower adherends are fixed as $\upsilon_1 = 0.293$ (steel) and $\upsilon_2 = 0.345$ (aluminum). For the adhesive layer, three thickness ratios ($h_0/h_2 = 0.2$, and 0.5) and two modulus ratios ($E_0/E_2 = 1/20$ and $1/10$) are adopted, and the Poisson's ratio is fixed at $\upsilon_0 = 0.4$ (thermosetting epoxy) in

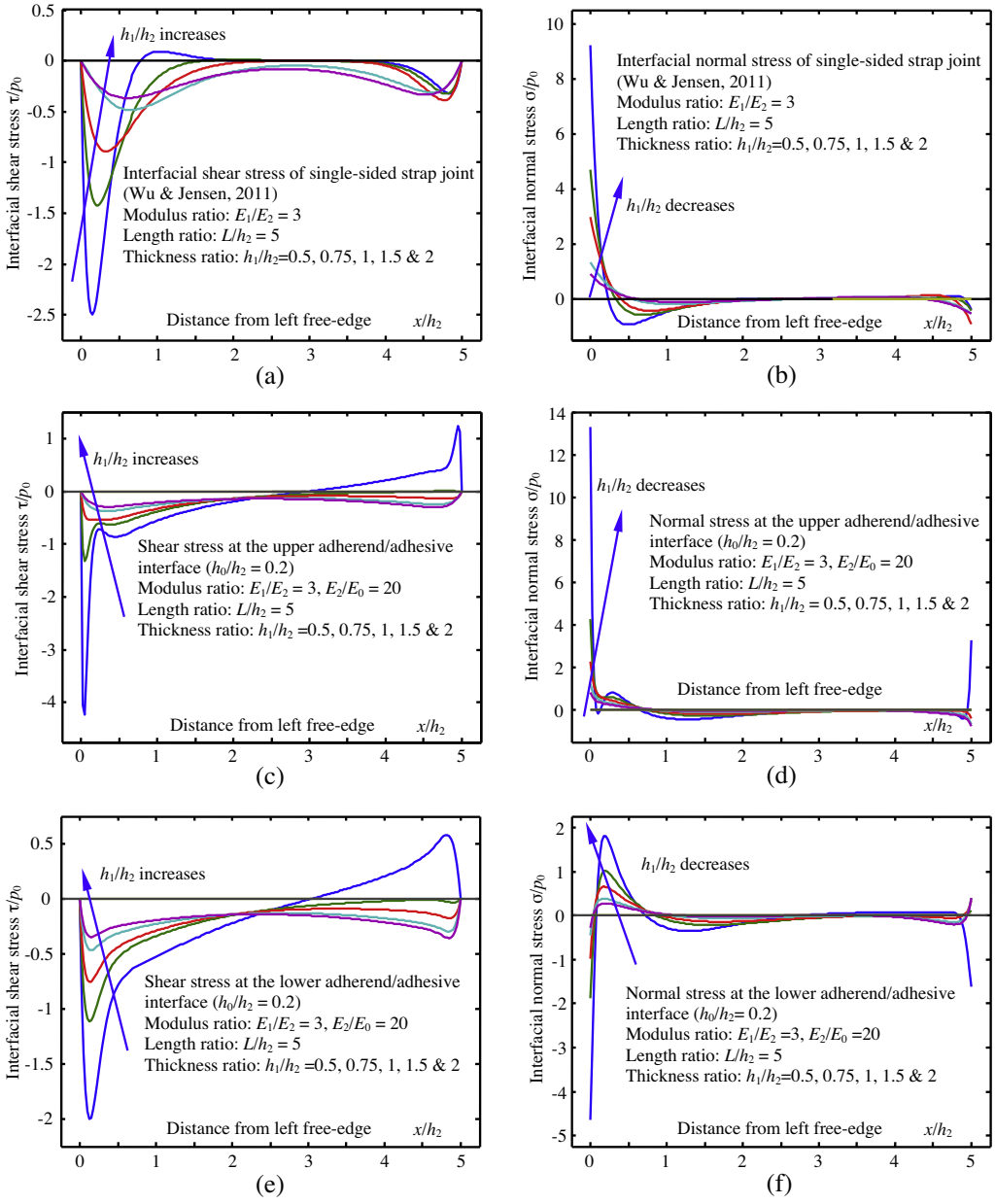


**Fig. 7.** Comparison of interfacial shear and normal stresses at the upper and lower adherend/adhesive interfaces with $E_2/E_0 = 20$ and $h_0/h_2 = 0.2$.

the calculations. The joint is treated in the state of *plane-stress*. Figs. 7–10 show variations of the dimensionless upper and lower interfacial shear stress $\tau/p_0$ and normal (peeling) stress $\sigma/p_0$ with the dimensionless distance $x/h_2$ from the joint mid-span to the right adherend end at five adherend thickness ratios ($h_1/h_2$ = 0.5, 0.75, 1.0, 1.5, and 2.0), two adhesive thickness ratios ($h_0/h_2$ = 0.2 and 0.5), and two adhesive modulus ratios ($E_0/E_2$ = 1/10 and 1/20), respectively. For the purpose of comparison, the interfacial shear and normal stresses of a bonded single-sided strap joint without the adhesive layer are also simulated using the reduced method developed recently (Wu and Jenson, 2011) as shown in Fig. 7(a) and (b). In all the simulations, the shear stress components satisfy the shear-free condition at the adherend ends.

It can be observed from Fig. 7 that high interfacial shear and normal stress concentrations exist near the interior edges of the adherends. For both types of joints with and without the adhesive layer, due to the existence of a bending moment at the mid-span, as illustrated in Fig. 2(*b*), the peak value of interfacial normal stress at the interior edges is much larger than that of the shear stress in all the cases under this study, which is also validated by FEM in a special case as shown in Fig. 4. In addition, the peak value of the shear stresses at both the upper and lower surfaces of the adhesive layer decreases with increasing adherend thickness ratio $h_1/h_2$. Except for the case of $h_1/h_2$ = 0.5, the shear stresses at the upper and low surfaces of the adhesive layer have close variation along the interface. Also, the peak value of the normal stresses at the upper and lower interfaces have very close varying trend; these interfacial normal stresses increase rapidly with the decrease of adherend thickness ratio $h_1/h_2$. Such observation implies that a thicker upper adherend (i.e., the cover layer with larger flexural rigidity) can suppress the joint deflection and flexural stress and therefore suppress the debonding failure. The larger normal stress at the upper surface of the adhesive layer implies that the debonding failure would be pliable to start along the upper adherend/adhesive interface.

The observed varying trends of both the interfacial shear and normal stresses hold for all the cases under this investigation. Furthermore, by comparison of stresses in Fig. 7 with those in Figs. 8-10, it can be concluded that when letting only one parameter vary and fixing the rest parameters, both the interfacial shear and normal stresses decrease noticeably with increasing thickness of the adhesive layer and also decrease slightly with decreasing elastic modulus of the adhesive layer for the parameters utilized in this study. This observation can be understood that the thicker and more complaint adhesive layer could provide larger deformation to accommodate the mismatching deformations between the upper and lower adherends and therefore decreases the interfacial stresses.

Therefore, the above scaling analysis could provide a clear picture on how the joint geometries and material properties influence the interfacial shear and normal stresses of the ABJs. These scaling results can be used to guide reliable and rational structural design and strength and failure analysis of ABJs. Furthermore, based on the interfacial stress functions (71a)-(71d), though approximately, the entire stress field in the ABJs can be determined in high accuracy using the relations formulated in Section 2.3. Consequently, it needs to be emphasized that the theoretical formulation of the present stress-function variational method is based on *Euler–Bernoulli* beam theory and linear elasticity, and no further assumptions are introduced in the above process. The only limitation of the present ABJ model is that the axial stresses in the adherends and adhesive should be linearly varying. Therefore, the present theoretical modeling of stress field in ABJs is theoretically self-consistent; accuracy of the stress field of ABJs based on the present model only relies on the numerical process in solving the resulting

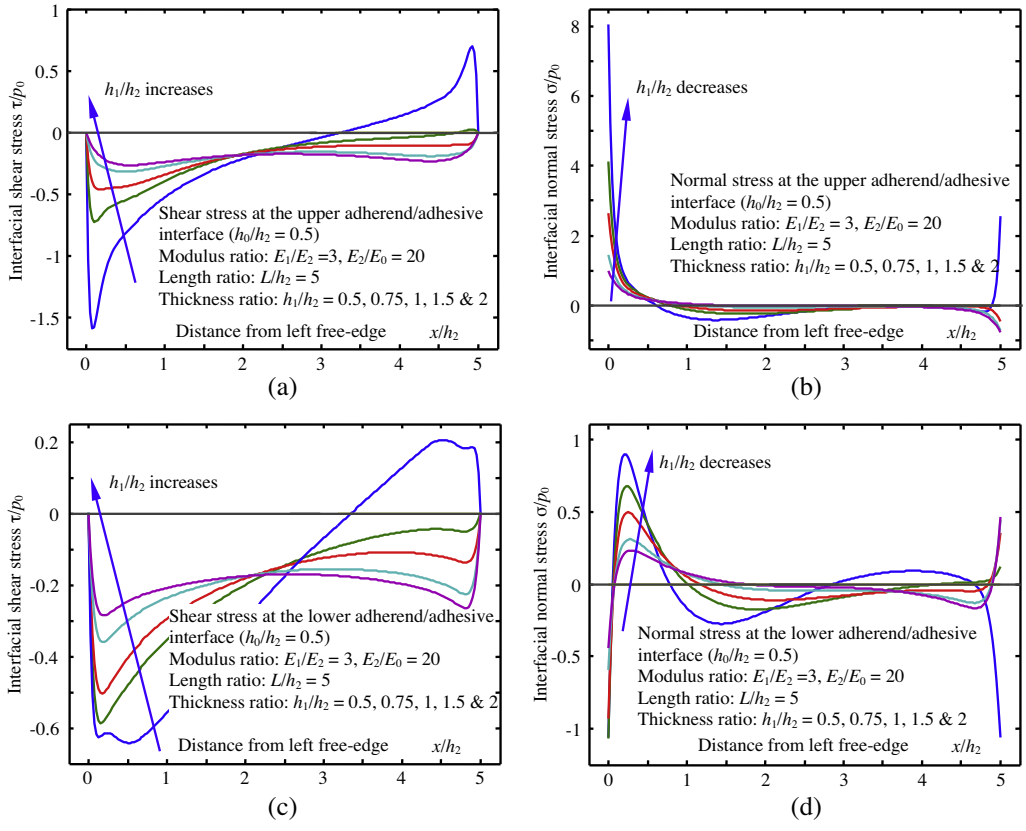


**Fig. 8.** Comparison of interfacial shear and normal stresses at the upper and lower adherend/adhesive interfaces with $E_2/E_0$ = 20 and $h_0/h_2$ = 0.5.

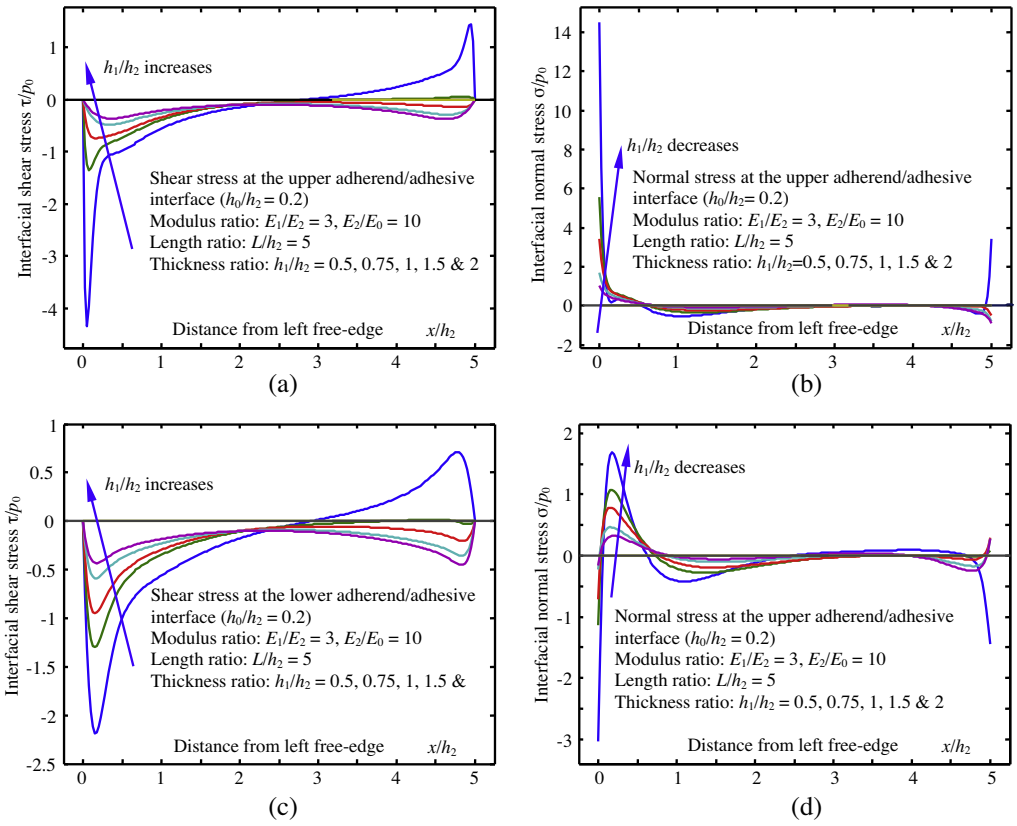


**Fig. 9.** Comparison of interfacial shear and normal stresses at the upper and lower adherend/adhesive interfaces with $E_2/E_0 = 10$ and $h_0/h_2 = 0.2$.

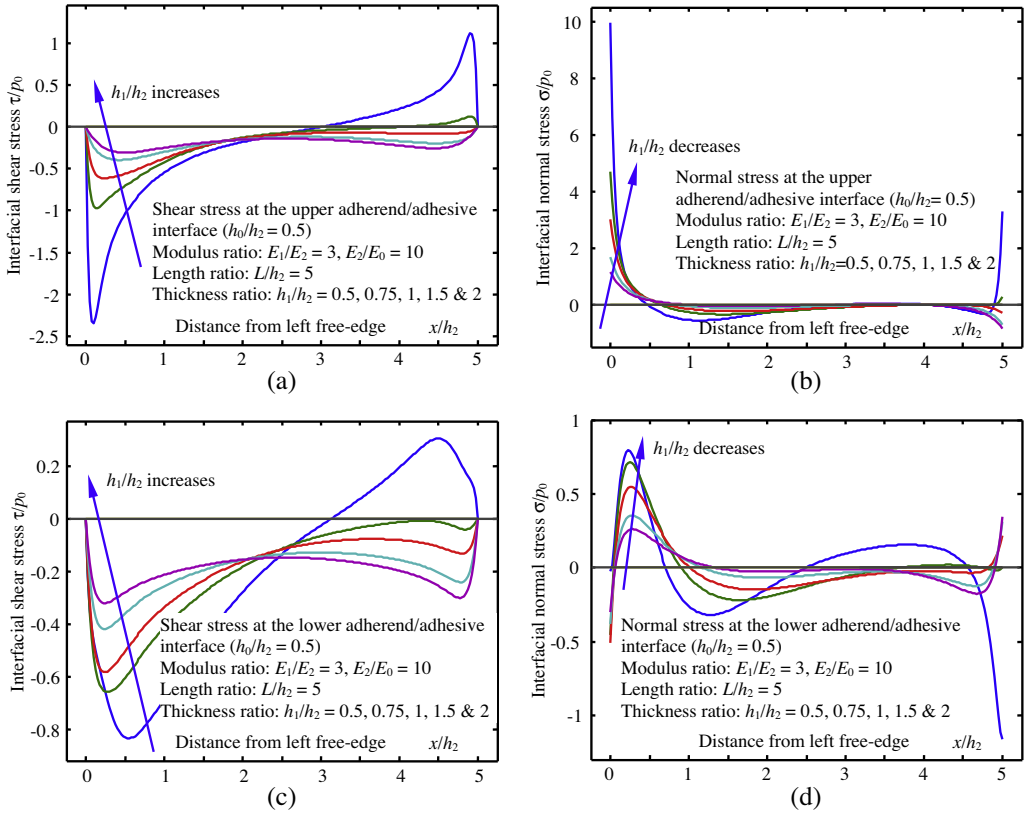


**Fig. 10.** Comparison of interfacial shear and normal stresses at the upper and lower adherend/adhesive interfaces with $E_2/E_0 = 10$ and $h_0/h_2 = 0.5$.

set of 16 simultaneous algebraic Eqs. (70a)-(70p), independent of the adhesive thickness and length.

## 4. Concluding remarks

A novel, general, self-consistent stress-function variational method has been successfully established for stress analysis of ABJs subjected to mechanical or thermomechanical loads. The modeling process was demonstrated in a special case of adhesively single-sided strap joint. During the theoretical formulation, at each adherend/adhesive interface of the ABJ, two unknown interfacial shear and normal stress functions were introduced. Therefore, the entire stress filed of the ABJ can be expressed consistently into such four interfacial stress functions on the two interfaces within the framework of *Euler–Bernoulli* beam theory and linear elasticity. The governing set of four ODEs has been obtained by evoking the theorem of minimum complementary strain energy and solved by eigenfunction method successfully. Such a set of governing ODEs can be considered as the characteristic equations for all ABJs made of three layers, which, by slightly modifying the traction BCs, can also be conveniently broadened for determining stresses in a wide family of three-layer systems including adhesively bonded single-lap joints, composite joints, etc. The advantages of the present formulation include its generality and the stress-field solution satisfying all the multiple traction BCs at the adherend ends and across the interfaces. The present work has been validated by FEA, and the scaling analysis of the present study has indicated very useful guidelines in stress analysis and structural design of ABJs.

In addition, though dealing with a classic engineering mechanics problem in ABJs, the present study can improve the efficiency and accuracy of stress analysis in ABJs and therefore has practical applications in engineering. Consequently, the theoretical formalism of stress-function variation developed in the present work can be conveniently generalized to solve a variety of strength and mechanical durability problems of adhesively bonded structures and layered materials including recently developed flexible electrics, etc.

## Acknowledgments

Partial support of the research by the NSF, NASA EPSCoR (NASA Grant # NNX07AK91A, seed grant: 43500-2490-FAR018640), NDSU Development Foundation, and NDSU Faculty Research Initiative Grant is gratefully appreciated.

## References

Beer, F.P., Johnston Jr., E.R., DeWolf, J.T., Mazurek D.F., 2009. Mechanics of Materials, fifth ed. McGraw Hill, New York.
Chen, D., Cheng, S., 1983. An analysis of adhesive-bonded single-lap joints. J. Appl. Mech. Trans. ASME 50, 109–115.
Chen, W.T., Nelson, C.W., 1979. Thermal stress in bonded joints. IBM J. Res. Develop. 23, 179–188.
da Silva, L.F.M., das Neves, P.J.C., Adams, R.D., Spelt, J.K., 2009a. Analytic models of adhesively bonded joints-part I: Literature survey. Int. J. Adhes. Adhes. 29, 319–330.
da Silva, L.F.M., das Neves, P.J.C., Adams, R.D., Wang, A., Spelt, J.K., 2009b. Analytic models of adhesively bonded joints-part II: Comparative study. Int. J. Adhes. Adhes. 29, 331–341.
Davis, M., Bond, D., 1999. Principles and practices of adhesive bonded structural joints and repairs. Int. J. Adhes. Adhes. 19, 91–105.
Diaz, A.D., Hadj-Ahmed, R., Foret, G., Ehrlacher, A., 2009. Stress analysis in a classical double lap, adhesively bonded joint with a layerwise model. Int. J. Adhes. Adhes. 29, 67–76.
Delale, F., Erdogan, F., Aydinoglu, M.N., 1981. Stress in adhesively bonded joints: a closed-form solution. J. Compos. Mater. 15, 249–271.
Eischen, J.W., Chung, C., Kim, J.H., 1990. Realistic modeling of edge effect stresses in bimetallic elements. J. Electron. Packag. 112, 16–23.
Goland, M., Reissner, E., 1944. The stresses in cemented joints. J. Appl. Mech. Trans. ASME 11, A17–A27.
Hadj-Ahmed, R., Foret, G., Ehrlacher, A., 2001. Stress analysis in adhesive joints with a multiparticle model of multilayered materials (M4). Int. J. Adhes. Adhes. 21, 297–307.
Higgins, A., 2000. Adhesive bonding of aircraft structures. Int. J. Adhes. Adhes. 20, 367–376.
Hutchinson, J.W., Suo, Z., 1992. Mixed mode cracking in layered materials. Adv. Appl. Mech. 29, 63–191.
Kim, D.H., Rogers, J.A., 2008. Stretchable electronics: materials strategies and devices. Adv. Mater. 20, 1–6.
Kumar, S., Scanlan, J.P., 2013. On axisymmetric adhesive joints with graded interface stiffness. Int. J. Adhes. Adhes. 41, 57–72.
Lee, J., Kim, H., 2005. Stress analysis of generally asymmetric single lap adhesively bonded joints. J. Adhes. 81, 443–472.
Lu, N.S., Yoon, J., Suo, Z.G., 2007. Delamination of stiff islands patterned on stretchable substrates. Int. J. Mater. Res. 98, 717–722.
Mortensen, F., Thomsen, O.T., 2002. Analysis of adhesive bonded joints: a unified approach. Compos. Sci. Tech. 62, 1011–1131.
Park, S.Y., Choi, W.J., Choi, H.S., Kwon, H., Kim, S.H., 2010. Recent trends in surface treatment technologies for airframe adhesive bonding processing: a review (1995–2008). J. Adhes. 86, 192–221.
Racker, B., 2004. Bonding processes in airbus in: 2004 FAA Workshop on Adhesive Bonding, Sussex, UK, (available at http//:www.niar.wichita.edu).
Ru, C.Q., 2002. Interfacial thermal stresses in bimaterial elastic beams: modified beam models revisited. J. Electron. Packag. 124, 141–146.
Suhir, E., 1989. Thermally induced interfacial stresses in elongated bimaterial plates. Appl. Mech. Rev. 42, S253–S262.
Suo, Z.G., 2003. Reliability of interconnect structures. In: Gerberich, W., Yang, W. (Eds.), Interfacial and Nanoscale Failure. Elsevier, Amsterdam, Netherland, pp. 265–324.
Suo, Z.G., 2012. Mechanics of stretchable electronics and soft machines. MRS Bull. 37, 218–225.
Suo, Z.G., Hutchinson, J.W., 1990. Interface crack between two elastic layers. Int. J. Fract., 1–18.
Sun, J.Y., Lu, N.S., Oh, K.H., Suo, Z.G., Vlassak, J.J., 2013. Islands stretch test for measuring the interfacial fracture energy between a hard film and a soft substrate. J. Appl. Phys. 113. Article No. 223702.
Tomblin, J., Davies, C., 2004. Bonded structures industry survey in: 2004 FAA Workshop on Bonded Structures, Seattle, WA, 2004, June.
Tsai, M.Y., Hsu, C.H., Han, C.N., 2004. A note on Suhir's solution of thermal stresses for a die-substrate assembly. J. Electron. Packag. Trans. ASME 126, 115–119.
Volkersen, O., 1938. Die Nietkraftverleitung in zugbeanspruchten Nietverbindungen mit konstanten Laschenquerschnitten. Luftfahrtforschung 15, 41–47.
Wu, X.F., Dzenis, Y.A., 2002. Closed-form solution for a mode-III interfacial edge crack between two bonded dissimilar elastic strips. Mech. Res. Commun. 29, 407–412.
Wu, X.F., Dzenis, Y.A., Fan, T.Y., 2003. Two semi-infinite interfacial cracks between two bonded dissimilar elastic strips. Int. J. Eng. Sci. 41, 1699–1710.
Wu, X.F., Jenson, R.A., 2011. Stress-function variational method for stress analysis of bonded joints under mechanical and thermal loads. Int. J. Eng. Sci. 49, 279–294.
Wu, X.F., Lilla, E., Zou, W.S., 2002. A semi-infinite crack between two bonded dissimilar elastic strips. Arch. Appl. Mech. 72, 630–636.
Yousefsani, S.A., Tahani, M., 2013a. Accurate determination of stress distribution in adhesively bonded homogenous and heterogeneous double-lap joints. Eur. J. Mech. A 39, 197–208.
Yousefsani, S.A., Tahani, M., 2013b. Analytic solution for adhesively bonded composite single-lap joints under mechanical loadings using full layerwise theory. Int. J. Adhes. Adhes. 43, 32–41.
Yu, H.H., Hutchinson, J.W., 2001. Edge effects in thin film delamination. Acta Mater. 49, 93–107.
Yu, H.H., Hutchinson, J.W., 2003. Delamination of thin film strips. Thin Solid Films 423, 54–63.
Zhao, B., Lu, Z.H., Lu, Y.N., 2011. Closed-form solutions for elastic stress–strain analysis in unbalanced adhesive single-lap joints considering adherend deformations and bond thickness. Int. J. Adhes. Adhes. 31, 434–445.